University of Alberta

Harmonic Impedance and Harmonic Source Determination Based on Field Measurements

by

Edwin Enrique Nino Hernandez

A thesis submitted to the Faculty of Graduate Studies and Research
in partial fulfillment of the requirements for the degree of

Master of Science

Department of Electrical & Computer Engineering

Spring 2010
Edmonton, Alberta

Examining Committee

Dr. Wilsun Xu, Department of Electrical & Computer Engineering

Dr. Michael Buro, Department of Computing Science

Dr. Tongwen Chen, Department of Electrical & Computer Engineering

I dedicate this thesis in memory of

my grandmother Paulina and my uncle Jhon Fredy

Abstract

Harmonic impedance characterizes the voltage response of a power system when it is subjected to the influence of high-frequency currents. The impedance is a key parameter of a power network and must be known to diagnose power system problems caused by high-frequency disturbances and to design disturbance-mitigation measures.

Unfortunately, determining an operating power system's harmonic impedances is very difficult; they must be measured when the system is energized. In fact, how to measure a power system's high-frequency impedances has been a challenging and frequent research topic in the power engineering field.

This thesis presents a measurement methodology that can determine the harmonic impedances and sources at both sides of utility-customer interface. This methodology is applicable to single-phase three-wire systems under energized conditions. A potential application of the method is to determine the harmonic contributions of the supply system and its customers at the interface points.

Acknowledgement

I am grateful to all who helped me to complete this thesis. The expert guidance and advice from my supervisor, Dr. Wilsun Xu, made its completion possible. I also give special thanks also to Dr. Sami Abdulsalam for his constructive feedback in our technical discussions. I also thank my fellow students in the Power Disturbance and Signaling Research Lab for providing a supportive and friendly environment. I especially thank Hooman Erfania, who was always keen to share his knowledge and experience. As well, I would like to thank my parents and my sister in Colombia, and, here in Canada, my wife, Piedad, and my son, Mathias, for their patience and understanding. They have played and will always play a decisive role in giving me the two most important things in my life, *love* and *happiness*. Finally, I thank God for His love and care in enabling me to achieve the most important goals in my life.

Table of Contents

List of Tables

List of Figures

Chapter 1

Introduction

In ideal conditions, power electricity should be delivered under perfect parameters to all customers. However, due to the complexity and diverse effects of power systems, these optimal conditions cannot be fully satisfied, and, as a result, the quality of the supplied power is compromised.

In recent years, the proliferation of power electronic loads has substantially increased, so the quality of electrical power has become an important subject for power systems. Nowadays, equipment is more sensitive to power quality issues and due to high-efficiency constraints, maintaining low harmonic level is critical. Transients, voltage sags, phase imbalance and harmonics, among others factors, are examples of the power quality concerns, not only for utilities but also for customers.

This introductory chapter provides a brief overview of power quality focused on harmonics in electrical systems. These concepts are explored in the first three sections of this chapter. Special mention is made of harmonic impedance and network frequency response in Section 1.4. Harmonic sources are described in Section 1.5. Finally, the scope, the objectives and a brief outline of this thesis are presented in Section 1.6.

1.1 Power Quality & Harmonics

The concept of power quality has been used in different ways depending on the applicability and/or scope of the analysis desired and on who does this analysis. From the utilities' and regulators' points of view, power quality is related to how to maintain voltage as a sinusoid at a rated magnitude and frequency [1]. For an equipment manufacturer, power quality refers to the characteristics of the power supply that enable the equipment to work properly.

The *IEEE Standard Dictionary of Electrical and Electronics Terms* defines power quality as "the concept of powering and grounding sensitive electronic equipment in a manner that is suitable to the operation of that equipment" [2]. Power quality is also defined as "[a]ny power problem manifested in voltage, current, or frequency deviations that result in failure or misoperation of customer equipment" [3]. In this sense, the ultimate gauge of power quality is its ability to ensure that an electrical apparatus functions correctly.

Power quality assessment is difficult and is determined mainly by the performance of the end-user equipment. Power quality is poor when the electric power is inadequate for customer needs. One difficulty is that the power supply system can control only the quality of the voltage, but not the currents that the loads draw. As a result, some of the power quality monitoring analyses are focused on keeping the supply voltage within certain limits.

A simple example of a power quality problem occurs when an AC power system, which is designed to operate at a sinusoidal voltage of a given frequency [50 or 60 Hz] and magnitude, presents considerable deviation in the waveform magnitude and frequency. Deviations result from many causes, such as short circuits, which result in voltage sags. Another example occurs when distorted

currents from harmonic-producing loads also distort the voltage as they pass through the system impedance. System and load impedances are the main focus of this thesis and their concepts are presented in the upcoming sections.

The economic impact of poor power quality is significant. Modern and high-efficiency apparatuses (in many cases, costly equipment) are very sensitive, and their malfunction may result in thousands of dollars of losses in key manufacturing facilities, for instance. Utilities are also economically concerned about power quality issues. In deregulated and competitive schemes, providing reliable and high-quality power is essential to attract and keep new customers.

1.2 Power quality disturbances

Identifying and classifying the distortions and, therefore, the deviations of ideal power characteristics are essential in order to correctly assess power quality analysis. References [3] and [4] describe power quality problem in detail. These disturbances can be classified into

- Transients
- Short- and long-term variations
- Frequency variations
- Waveforms distortions

The scope of this thesis is related to waveform distortions, specifically harmonics. These distortions can increase power losses and create interference in communication systems. Furthermore, control and protection actions can also be affected by harmonics. Next section presents these harmonic distortions in more detail.

1.3 Harmonics

1.3.1 Definition

The periodic characteristics of voltage and current are very important in power quality analysis. A sinusoidal voltage or current function can be decomposed into the sum of the fundamental and harmonic components, which are also sinusoidal components of the original periodic wave having a frequency that is an integral multiple of the fundamental frequency.

Thus, *harmonics* are steady-state components of a distorted periodic voltage or current waveform whose frequencies are integer multiples of the fundamental frequency (50 or 60 Hz). Due to the characteristics of this type of distortions, Fourier analysis is a useful tool to compute harmonics.

Harmonics are one of the major power quality problems in power systems. Harmonic distortion is caused by nonlinear devices in which the current is not proportional to the applied voltage. These distortions can be determined by frequency spectra, which contain the magnitude and phase angle for each harmonic component.

In most power system applications, waveforms have both positive and negative half cycles, and, as a result, only odd harmonics are considered. Usually, the higher-order harmonics are negligible for power system analysis. Due to the characteristics of the problem tackled in this work, collecting sufficiently accurate data to model power systems at high frequencies is difficult, so harmonics only up to the 13^{th} order are considered. This issue will be discussed in detail in the subsequent chapters.

1.3.2 Harmonic Indices

Harmonic indices have been developed to assess the service quality of a power system with respect to the harmonic distortion levels. These indices are measures of the effective value of a waveform and can be applied to both the current and the voltage [5-7]. Several indices are available for harmonic analysis; however, the two most commonly used (also in this thesis) are the total harmonic distortion and the total demand distortion:

- Total Harmonic Distortion (THD): Is the ratio of the RMS value of the sum of the individual harmonic amplitudes to the RMS value of the fundamental frequency expressed in percent. Equations (1-1) and (1-2) show the total harmonic distortion for voltage and current respectively:

$$THD_V = \frac{\sqrt{\sum_{h=2}^{\infty} V_h^2}}{V_1} \qquad (1\text{-}1)$$

$$THD_I = \frac{\sqrt{\sum_{h=2}^{\infty} I_h^2}}{I_1}, \qquad (1\text{-}2)$$

where h represents the harmonic order.

- Total Demand Distortion (TDD): Is the total harmonic current distortion defined by the ratio of the RMS value of the sum of the individual harmonic amplitudes to the maximum or rated demand load current I_L as shown in the following expression:

$$TDD_I = \frac{\sqrt{\sum_{h=2}^{\infty} I_h^2}}{I_L}. \qquad (1\text{-}3)$$

1.4 Harmonic Impedance

In harmonic analysis, the *impedance* is a key characteristic parameter in power systems. Electric power flowing from the generation units to the final customers experience voltage drops due to the impedance. If this concept is expanded to include high frequencies (again, integer multiples of the fundamental frequency), it is called *harmonic impedance*. In other words, harmonic impedance characterizes the voltage response of a power system when it is subjected to the influence of high-frequency currents.

Two types of impedances are used in harmonic studies: the impedance of a supply system network and the impedance of a load. Figure 1-1 presents a typical scenario where harmonic impedance measurement is needed. The interface point between the network and the customer is called the *point of common coupling* (PCC). The upstream system-side and downstream load-side equivalents at the interface point can be represented as shown in Figure 1-2.

In power systems analysis, the equivalent system impedance is also known as the short-circuit impedance and at the fundamental frequency is primarily inductive; however, shunt capacitors may affect this characteristic. At this point, the load of interest can be represented by the load-side impedance, also known as the customer impedance, which can be sensed by acquiring the voltage and current data. Revenue meters are usually located at the PCC.

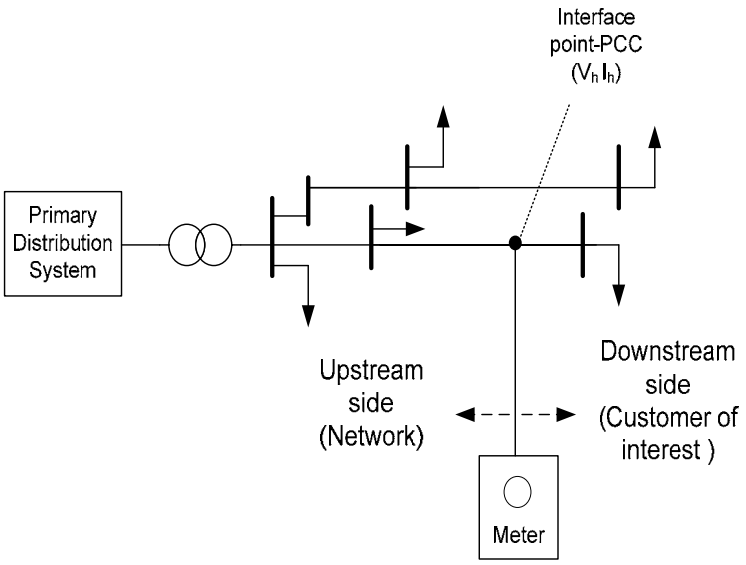

Figure 1-1 Distribution system configuration for harmonic impedance analysis purposes at PCC.

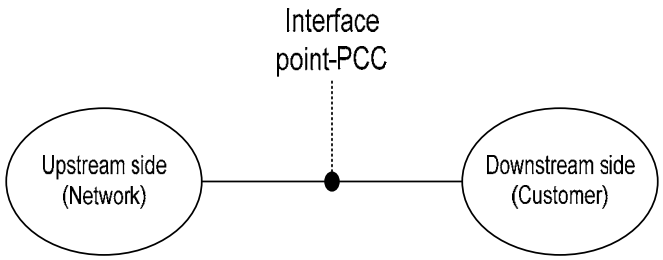

Figure 1-2 Equivalent interpretation of distribution system at the interface point.

1.4.1 Importance of Harmonic Impedance

The harmonic impedance must be known to accurately represent power system frequency responses and to design harmonic-mitigation schemes. A system's harmonic propagation cannot be accurately simulated or predicted without impedance information. For instance, harmonic impedance is needed in harmonic filter design and harmonic source determination. This parameter plays a significant

role in harmonic analysis not only for utilities but also for different types of customers.

The interaction of harmonic sources with the system impedance may negatively affect the performance in the electrical network. As a result, the harmonic impedance is a key parameter affecting the system response characteristics and is a critical element in determining the harmonic voltages resulting from harmonic current emissions.

1.4.2 Problem Description

Figure 1-3 shows the equivalent representation of the power system of Figure 1-1 and illustrates the problem of harmonic impedance measurement. This problem can be defined as how to determine the harmonic impedances for the customer and the network, Z_C and Z_N respectively.

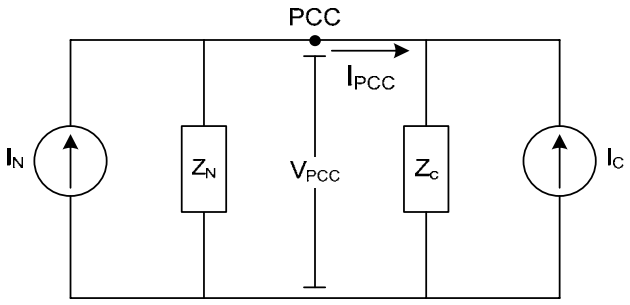

Figure 1-3 Current source equivalent circuit for harmonic analysis.

Unfortunately, calculating the impedances in an operating power system is very difficult. Because of practical limitations and service-continuity reasons, these parameters cannot be measured by shutting down the power system. These parameters should be measured when the system is energized. Moreover, the system's dynamic nature, i.e., the changes in loads, network elements and system configurations, makes impedance calculations a challenging task.

1.4.3 Network Frequency Response

In the frequency domain, the impedance is a complex value that can be decomposed into the resistance and reactance (the impedance's real and imaginary part, respectively). Although in some cases, the system's equivalent impedance is assumed to be purely reactive, a more realistic approach must consider the resistive part in the presence of smaller transformers and especially for low voltage systems, so this approach will be followed in this thesis. For the harmonics, the inductive part of the impedance is linearly affected by the frequency while the resistive part generally remains constant for low harmonic orders. Figure 1-4 presents a typical frequency response (assuming no presence of resonances or capacitor effects) of the system impedance.

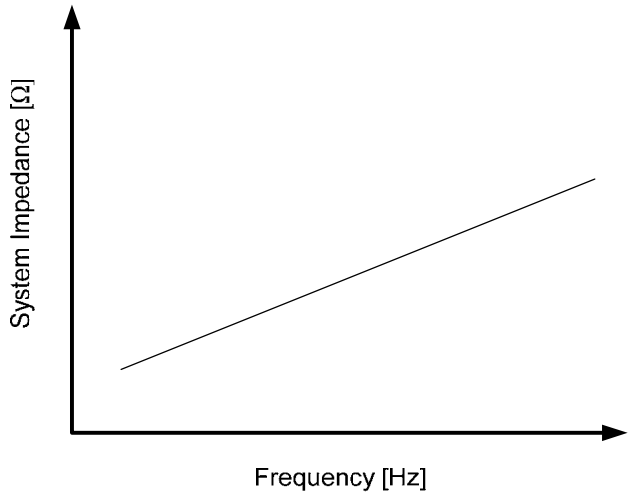

Figure 1-4 Frequency response of system impedance. Simple case.

The work presented in this thesis focuses on the frequency domain by identifying the response of the power system at each harmonic frequency.

1.5 Harmonic Sources

In harmonic analysis, the generating elements of the harmonics, i.e. the harmonic sources, must be identified and characterized. Non-linear electrical loads are known to be the major sources of power network distortion. Most nonlinear

loads are located within end-user facilities, and the highest voltage distortion levels occur close to the harmonic sources. This problem is not new. Earlier examples of harmonic sources were arc furnaces, fluorescent lamps, saturated transformers and rotating machines, which were responsible for transmission line and capacitor malfunctions. More recently, power electronic devices have become another important source of harmonic distortions. The number of harmonic-producing loads has increased noticeably, increasing the need to improve the management of harmonic problems. These distortions are present in almost all type of customers.

Commercial and residential loads are characterized by a large number of small harmonic-producing loads. These facilities present equipment with fluorescent lights with electronic ballasts; adjustable-speed drives for the heating, ventilation, and air-conditioning loads; elevator drives; and sensitive electronic equipment supplied by switching single-phase power supplies. The voltage distortion levels depend on both the circuit impedances and the overall harmonic current distortion.

Moreover, industrial facilities are characterized by the extensive application of nonlinear loads, such as power converters and arcing devices. These loads can make up a significant portion of the total facility loads and inject harmonic currents into the power system, causing harmonic distortion in the voltage.

Harmonic sources are generally considered to be injection sources in the linear network models. For most harmonic studies, harmonic sources are modeled as simple sources of harmonic currents or, more accurately, when they are in parallel with harmonic impedances (such models are known as Norton equivalents), as shown in Figure 1-3. This model is explored and estimated by using measurements in Chapter 6. Determining the response of the power system is

essential to analyze the impact of the nonlinear load on the harmonic voltage distortions.

1.6 Proposed research

Based on the general concepts explained in this chapter, such as power quality disturbances and harmonic analysis, this thesis is focused on determining *harmonic impedances* and *harmonic sources* as key parameters in power quality systems. The analyses are performed in the frequency domain.

The accurate estimation of harmonic impedance is fundamental in assessing harmonic limits. Furthermore, harmonic impedance studies are an important stepping stone for developing potential applications such as harmonic sources determination and harmonic contributions.

The objective of this thesis is to develop a harmonic impedance determination scheme for power systems under energized conditions. Several methods available in the literature are developed for three-phase systems and by assuming balanced system conditions; these approaches are presented in Chapter 2. However, they are not readily applicable to measure harmonic impedances in single-phase three-wire systems. The approach that can do so is intended to calculate impedances at the utility-customer interface in such systems. A scheme for this approach will be developed based on an efficient combination of existing and proposed new invasive methods, which will be extensively analyzed in Chapters 3, 4 and 5.

Harmonic impedance determination is extensively described in the next chapter. This thesis discusses four major topics: (1) impedance measurement techniques and the measurement scheme at the utility-customer interface point, (2)

utility-side harmonic impedance for single-phase systems, (3) customer-side harmonic impedance for the same type of configuration, and (4) characterization of harmonic sources based on harmonic impedance results.

Chapter 2

Impedance measurement techniques

System impedance is a key parameter of a power network and must be known in order to diagnose power system problems caused by high-frequency disturbances and to design disturbance-mitigation measures.

Unfortunately, determining an operating power system's harmonic impedances is very difficult; they must be measured when the system is energized. In fact, how to measure a power system's high-frequency impedances has been a challenging and frequent research topic in the power engineering field.

2.1 Introduction

Two approaches are used to obtain impedance information: one based on modeling and another based on measurements. The identification and modeling of impedance and other power system components has been documented in [8] and [9]. Nevertheless, impedances obtained by modeling are usually not very accurate, and the available information is limited. On the other hand, measuring impedances gives more accurate results. However, doing so is a difficult task. Impedances must be measured under energized conditions due to practical limitations and service continuity restrictions. Moreover, a system's dynamic nature, i.e., changes in loads, network elements, and system configurations, makes impedance measurement difficult.

This chapter describes the measurement techniques available in the literature. Transient and steady-state methods are fully explained. The research objectives of this thesis are summarized in the final section.

2.2 Literature review

Although several harmonic impedance determination methods have been proposed in the literature, no consensus exists, in terms of cost, simplicity and implementation. Each of them has advantages and disadvantages. A comprehensive harmonic determination methodology that combines the different advantages of existing methods is needed. Based on the available methods to measure harmonic impedance, Figure 2-1 show how they can be classified into non-invasive and invasive methods.

Non-invasive methods use natural variations of harmonic voltages and currents to measure harmonic impedances. These methods usually provide inaccurate results if no predominant harmonic distortion is present in a system. Without enough harmonic variations, the results are meaningless. Invasive methods usually generate good results, so the proposed thesis will focus on invasive methods.

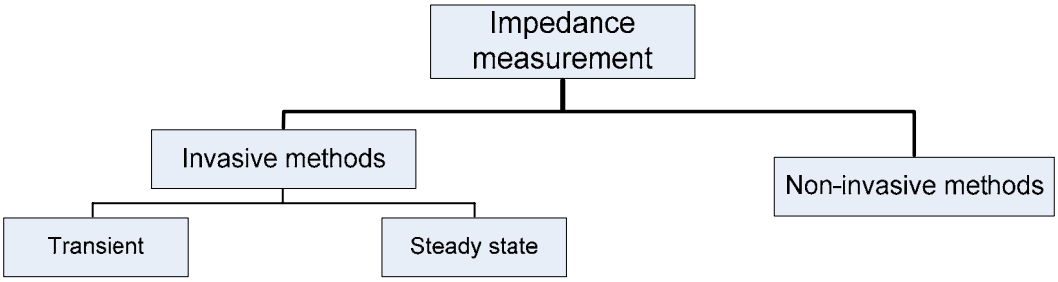

Figure 2-1 Impedance measurement methods.

Invasive methods create intentional changes in the power network and take measurements according to the harmonic voltage and current responses [13]. The basic principle of invasive methods is to use either the harmonic currents coming

from network equipment switching or the direct injection of harmonic currents. Invasive methods are intended to produce a disturbance in a system with enough energy for measurement purposes without affecting the network equipment operation. In general, invasive impedance measurement approaches can be separated into two types: transient based methods and steady-state based methods.

2.2.1 Transient methods

The applied disturbance in the system generates a transient process. Assuming that voltage and current waveforms are recorded by a high-speed data-acquisition device, the principle of these approaches is to use transient voltage and current data to obtain the harmonic impedance. Three major sources of disturbance are capacitor banks, transformers, and power electronic devices.

Switching a capacitor bank is approximately equivalent to causing an instantaneous short circuit; as a result, a current signal with a wide frequency range can be obtained. References [16-18] use capacitor switching to inject a current disturbance. Figure 2-2 shows the typical voltage and current transient waveforms due to a capacitor switching, and figure 2-3 presents the extracted transients and their respective frequency contents.

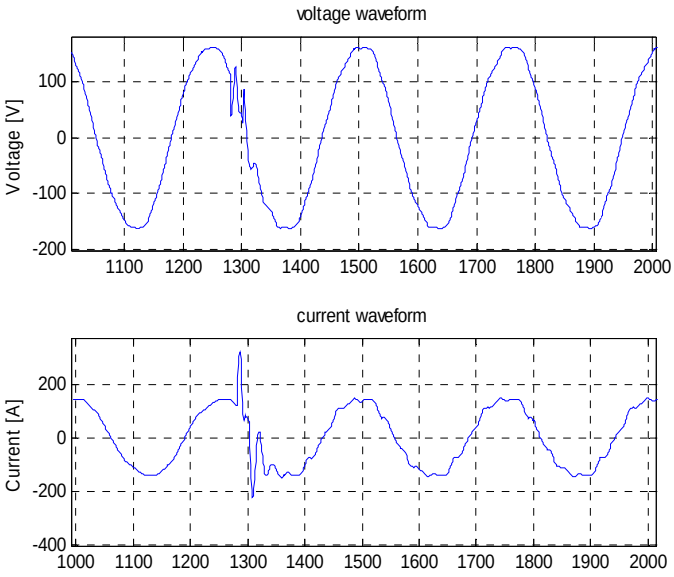

Figure 2-2 Voltage and current waveforms during a disturbance.

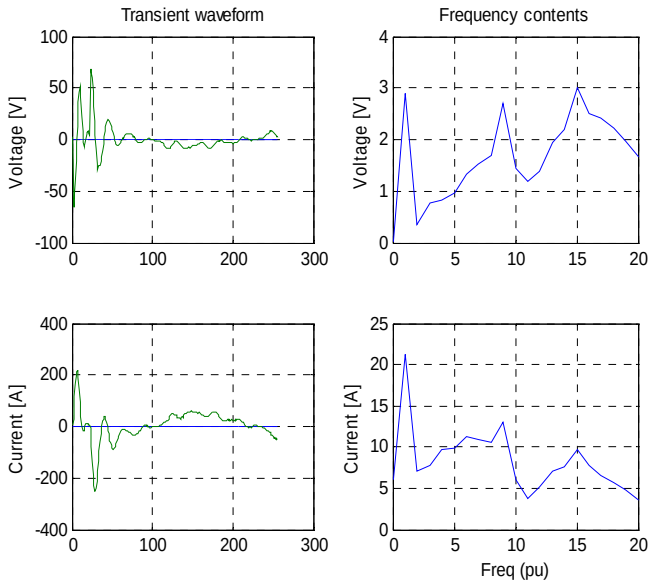

Figure 2-3 Transient waveforms and frequency contents.

Switching transformers can make them reach saturation. Transformer energization can generate high transient currents depending on the remanence and the switching moment. These currents, also known as *transient inrush currents*, have

wide frequency spectrum content with considerable magnitudes [12]. Their duration can be for a few cycles to a few minutes.

Other alternatives for sources of disturbance are power electronic devices. Reference [14] uses a power electronic converter to inject a controlled current spike in a system. Power electronic devices are able to control the firing angle (of thyristors in the case of converters) and therefore to control the switching process. Since the transients' strength depends on the switching moment, controlling their magnitudes and suitably disturbing the system for measurement purposes are desirable. The following are the most common transient methods used to measure harmonic impedance.

Direct method: The most common transient-based technique is called the *direct method*. Once a disturbance is exerted, the resultant transient voltage and current waveforms are captured. The Fourier transform is used to obtain the fundamental and harmonic magnitudes and phases of each signal. The harmonic impedance is simply calculated by using the traditional voltage-current ratio at each frequency:

$$Z(f) = \frac{V(f)}{I(f)} \quad . \tag{2-1}$$

One of the main concerns in practical applications is to guarantee feasible results after acquiring and processing a signal from the measurements. This approach is considerably affected by significant noise levels in the signals and by supply voltage distortions. A common practice for eliminating the supply voltage's influence is to collect two sets of data, one just previous to the injection of the spike current and another from the transient.

Some methods have been proposed to overcome noise problems and to improve results. For instance, [15] is concerned with the implementation of equipment and filtering. References [16-18] discuss correlation techniques and other statistical approaches.

Power spectral density: The power spectral density can be obtained from the correlation functions by using the Fourier transform. According to [19], correlation functions show how associated the signals are. Thus, [16] proposes calculating the high frequency impedances by using the voltage and current power spectra:

$$Z(f) = \frac{P_{VI}(f)}{P_{II}(f)}, \tag{2-2}$$

where $P_{VI}(f)$ is the cross-power spectrum of the voltage and current, which is obtained by applying the correlation's Fourier transform between the two signals. Similarly, the auto-power spectrum $P_{II}(f)$ is the Fourier transform of the current's auto-correlation.

The accuracy of the results is defined by a "squared coherence function," which provides a measure of the power in the system output (voltage) due to the input (current):

$$K_{VI}(f) = \frac{|P_{VI}(f)|^2}{P_{VV}(f)P_{II}(f)}. \tag{2-3}$$

This function is defined between 0 and 1, and only points with high coherence values are considered. This approach reduces the effect of noise and improves the accuracy of the impedance results.

Three-phase system approach: The previous approaches consider only one-phase-systems; however, most of real power networks are three-phase systems. In such systems, the mutual coupling effects must be considered. The mutual coupling has a significant impact since a transient in one phase can be affected by transients in the other phases. If this effect is not included, then harmonic impedance results can contain large errors. Reference [18] develops a technique to model these effects and to calculate harmonic customer impedances by using several capacitor-switching operations. For a three-phase configuration with phases *a*, *b* and *c* we have

$$\begin{bmatrix} V_a(f) \\ V_b(f) \\ V_c(f) \end{bmatrix} = \begin{bmatrix} Z_{aa}(f) & Z_{ab}(f) & Z_{ac}(f) \\ Z_{ba}(f) & Z_{bb}(f) & Z_{bc}(f) \\ Z_{ca}(f) & Z_{cb}(f) & Z_{cc}(f) \end{bmatrix} \cdot \begin{bmatrix} I_a(f) \\ I_b(f) \\ I_c(f) \end{bmatrix}, \tag{2-4}$$

where V and I are the voltages and currents per phase, respectively. The $\mathbb{Z}$ matrix involves self and mutual components in frequency domain. For each phase, three unknown impedance components have to be determined, e.g., for phase *a*: $\mathbb{Z}_{aa}$, $\mathbb{Z}_{ab}$ and $\mathbb{Z}_{ac}$. In order to determine these impedances, at least three close-trip operations are required. Reference [18] generates more than three close-trip operations and applies the least square method to determine the harmonic impedance. Thus, for phase *a* we have

$$[Z_a(f)]_{3x1} = \left[[I(f)]^T [I(f)]\right]^{-1}_{3x3} [I(f)]^T_{3xm} [V_a(f)]_{mx1}, \tag{2-5}$$

where $[Z_a(f)] = \begin{bmatrix} Z_{aa}(f) \\ Z_{ab}(f) \\ Z_{ac}(f) \end{bmatrix}$ and $[I(f)] = [I_a(f) \quad I_b(f) \quad I_b(f)]$.

m represents the number of close-trip operations. The bigger the number of operations (measurements), the more accurate the results are. Similar calculations can be applied for the other two phases.

2.2.2 Steady-state methods

Unlike transient-based methods, steady-state methods do not use transient signal information. Instead, pre- and post-disturbance voltage and current steady-state data are used. The following are the most common methods in the available literature.

Auxiliary impedance method [20]: This method uses an auxiliary impedance to create a new steady-state. Under no load conditions, the harmonic spectrum of the voltage (E_{noload}) is obtained. When the known auxiliary impedance is switched on, the voltage (E_{load}) and the current (I) harmonic spectra, i.e., the magnitudes and angles are obtained. Thus, phasor analysis can be used to compute the harmonic impedance as follows:

$$\begin{aligned} R_h &= \frac{E_h \cos\alpha - R_{h\,aux} \cdot I_h}{I_h} \\ X_h &= \frac{E_h \sin\alpha - X_{h\,aux} \cdot I_h}{I_h} \end{aligned}, \qquad (2\text{-}6)$$

where h represents the harmonic order, and α is the angle between E and I. This angle is a function of the pre- and post- switching conditions. This method has serious limitations because only impedances of the same harmonic orders as those existing in the distortion system can be measured.

Injecting harmonic current source [20]: This method is commonly used in some countries to measure harmonic impedances. The main idea is to inject a known harmonic current source (it can be obtained by switching a non-linear load); a pure

sinusoidal voltage waveform is assumed under no load conditions. The harmonic impedance can be calculated as

$$Z_N(f) = \frac{V(f)}{I(f)}. \tag{2-7}$$

This method's main disadvantage is that the supply has to be free from harmonic distortions under no load conditions. In addition, the harmonic impedance will not show other frequency components different from those of the harmonic's current source.

Hybrid method [20]: This method combines some of the procedures of the two previous methods. It considers measurements at the supply bus under no load conditions and uses a harmonic current injection to create the disturbance. From phasor analysis, the supply harmonic impedance is

$$\begin{aligned} R_h &= \frac{V_h \cos\beta_1 - E_h \cos\beta_2}{I_h} \\ X_h &= \frac{V_h \sin\beta_1 - E_h \sin\beta_2}{I_h} \end{aligned}. \tag{2-8}$$

Like the α angle in the auxiliary impedance method, β_1 and β_2 are angles depending on the pre- and post- switching conditions.

All those methods are based on assumptions of the harmonic content of the voltage supply. These assumptions are not always realistic and depend on the network's dynamic. The following method avoids the use of voltage supply data and provides more accurate results.

Pre- and post-disturbance using capacitor switching: Reference [21] presents an approach that modifies the injecting harmonic current source method. The steady-state measurement method uses the switching of a network component at the location where the network impedance is to be measured. Assuming that a shunt capacitor is available for switching, the method uses the pre- and post-disturbance steady-state waveforms of the voltages and currents at the PCC to estimate the impedances as follows:

$$Z_{eq-h} = -\frac{V_{h-post} - V_{h-pre}}{I_{h-post} - I_{h-pre}} = -\frac{\Delta V_h}{\Delta I_h}, \tag{2-9}$$

where ΔV and ΔI represent the subtraction of the pre- and post- disturbance voltage and current phasors, respectively. The subscript h represents the harmonic order.

Table 2—1 provides a comparison of the methods described in this literature review. In summary, steady-state methods are preferred in practical applications over transient-based methods, which need high-speed data-acquisition equipment. However, transient-based methods are still useful because transient signals contain abundant frequency components yielding accurate harmonic impedance results in a wide range of frequencies.

Table 2-1 Comparison of invasive harmonic impedance measurement methods.

Method		Advantage	Disadvantage
Transient		Wide range of frequency components. Very good detection of all harmonic orders depending on the disturbance source.	High-speed data acquisition equipment required. The presence of a switching is needed.
Steady-state	Auxiliary Impedance	Simplicity.	Not very accurate
	Injecting harmonic source	Most common in practice.	Assumes the supply is free of harmonic content. Influence of other sources in the network.
	Hybrid	Reasonable accuracy.	Assumes the supply is free of harmonic content. Influence of other sources in the network.
	Capacitor switching	Simplicity. Good accuracy.	A capacitor bank is needed. No control over switching moment.

2.3 Summary and research objectives

Table 2-2 summarizes which configurations have already been implemented by using invasive methods and which ones need to be implemented.

Table 2-2 Invasive methods for each configuration.

Configuration		Transient method	Steady-state method
Three-phase	Equivalent supply system	✓	✓
	Load	✓	✓
Single-phase three-wire	Equivalent supply system	×	×
	Load	×	×

(✓- done, × - not done)

The ultimate objective of the proposed thesis is to develop harmonic impedance measurement scheme for single-phase systems. The proposed

approaches are intended to calculate impedances at both sides of interface points. These approaches could be used as a stepping-stone to determine harmonic contributions and to characterize harmonic propagation in electric power systems.

Chapter 3

Utility-side harmonic impedance

Residential and commercial customers are usually supplied through single-phase transformers. The low voltage side of the transformer is a three-wire circuit with two phases and a neutral. This chapter presents a measurement method that can determine the harmonic impedances for this type of supply systems. The effectiveness of the proposed method has been demonstrated through simulation studies and field tests. A potential application of the method is to determine the harmonic sources of the supply system and its customers at the utility-customer interface points.

3.1 Introduction

This chapter presents the development of a method to measure the utility-side impedances in single-phase three-wire systems. This method's effectiveness has been demonstrated through simulation studies and field tests. The theoretical foundation of the proposed technique is based on [21]. However, this work must be improved and extended form the proposed measurement technique. The first aspect is to select an effective disturbance source and the second is to develop an impedance calculation algorithm for three-wire one-phase systems. The proposed technique develops an impedance calculation algorithm for three-wire single-phase systems, which are very common for residential and commercial customers at low voltage levels. The method uses a portable capacitor to create an operating condition change at the customer-utility interface point. Harmonic impedance information is extracted from the measured pre- and post-disturbance voltage and current waveforms. In addition, a potential application is presented to extend the method to harmonic source determination.

This chapter is organized as follows: Section 3.2 presents the problem of harmonic impedance determination for single-phase supply systems. Section 3.3 describes the proposed harmonic impedance measurement method and some important implementation issues. Simulation studies and field measurements are used to demonstrate the effectiveness of the proposed method in Sections 3.4 and 3.5 respectively. Finally, Section 3.6 presents the potential application of harmonic source determination for single-phase supply systems.

3.2 Problem Description

Many low voltage (LV) customers are supplied by a three-wire (two hot wires and a neutral) system as shown in Figure 3-1. The primary network consists of all medium voltage (MV) lines that come from the substation. For most residential customers, the distribution transformers are single-phase transformers connected between one phase and a neutral of the MV feeder. There are two hot branches carrying 120V with respect to the neutral and 240V between the branches at the secondary side of the distribution transformer. The transformers supply customers using a single-phase three-wire configuration (Figure 3-1b).

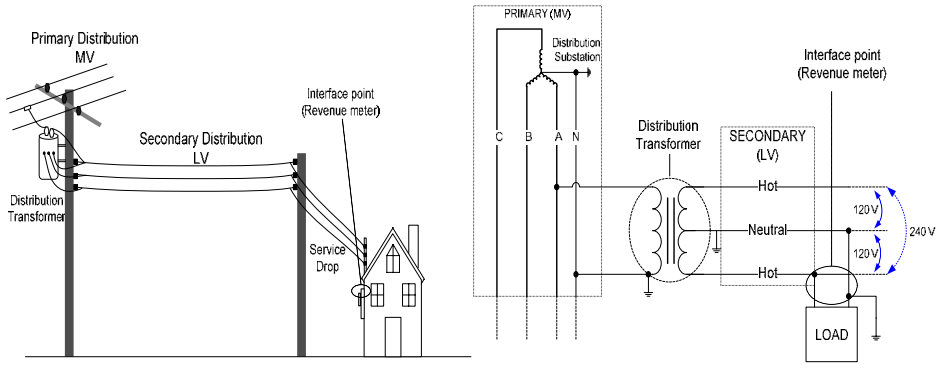

a. b.

Figure 3-1 Power distribution system for single-phase three-wire customers: a. Schematics and b. Circuit representation.

To determine the harmonic contributions of the customer and the supply at the revenue meter point, the equivalent circuit model of Figure 3-2 is proposed. In this model, there are harmonic current sources in both sides. The equivalent impedances are unknown. This chapter is focused on the selection of an effective disturbance source and the development of an impedance calculation algorithm for three-wire one-phase systems for the supply side. Finally a potential application is presented to estimate harmonic current source at the system side.

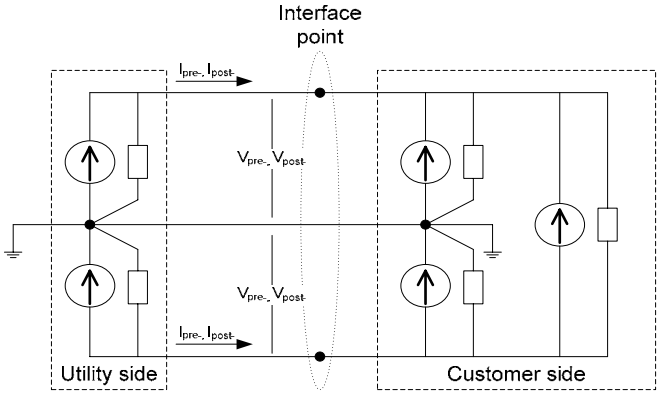

Figure 3-2 Harmonic source equivalent model for three-wire single-phase systems.

3.3 The proposed method

The method uses a portable capacitor to create an operating condition change at the customer-utility interface point. Harmonic impedance information is extracted from the measured pre- and post-disturbance voltage and current waveforms.

This work improves and extends the approach of [21]. The method uses pre- and post-disturbance steady-state waveforms of the voltages and currents at the interface point to estimate the impedances by using equation (3-1). Figure 3-3 shows the current source equivalent supply system seen from the interface point, where voltage and current are measured.

$$Z_{eq-h} = -\frac{V_{h-post} - V_{h-pre}}{I_{h-post} - I_{h-pre}} = -\frac{\Delta V_h}{\Delta I_h} \tag{3-1}$$

ΔV and ΔI represent the subtraction of pre- and post- disturbance voltage and current phasors respectively. The subscript h represents the harmonic order.

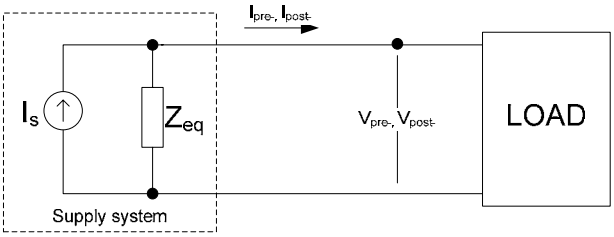

Figure 3-3 Equivalent circuit for one-phase systems. Current source model.

3.3.1 Source of disturbance

The basic method works only if a disturbance occurs at the customer side. Field experiences show that the naturally occurring disturbances caused by customer load switching are neither sufficient nor efficient for impedance estimation. Introducing disturbances during a test is more effective. Fortunately, doing so is not a difficult task due to the system's low voltage nature. In fact, extensive field experiences showed that a portable capacitor bank is sufficient. In addition to the advantages identified in the literature review, the other advantages of using a capacitor bank compared to other sources of disturbance are the following:

- LV capacitors are portable and easy to connect.
- They draw harmonic currents from the supply system and can create larger voltage and current changes.
- Since the capacitor energization period is very short (say 1 second.), a wide variety of AC capacitors with high farad values are available. The cost is very low.

Figure 3-4 illustrates the proposed capacitor bank arrangement. The capacitors are discharged through a 1kΩ resistor. The component values are selected based on the requirements to (1) produce sufficient voltage change, (2) cause an acceptable disturbance to customers, and (3) discharge quickly (less than 0.5sec) for fast repetitive switching. The switches of the capacitor elements are used to vary the capacitor bank's total size. A disturbance is introduced by connecting the main switch to the system. Figure 3-5 shows the sample voltage and current waveforms in branch *a* caused by the capacitor switching.

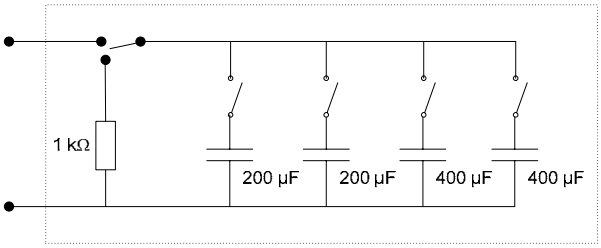

Figure 3-4 Capacitor bank as source of disturbance.

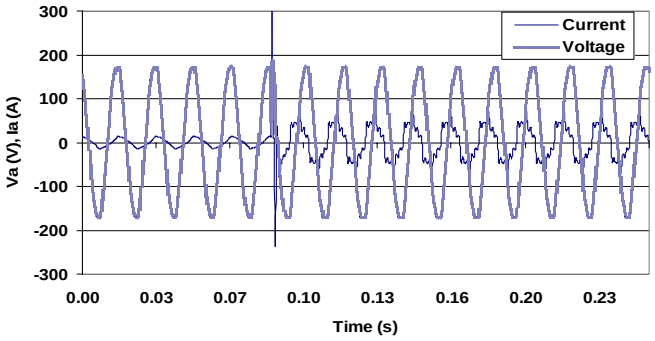

Figure 3-5 Load voltage and current.

Figure 3-5 reveals a voltage transient. Since its duration was very short, the transient was not found to have any adverse effects on the loads. If the transient had been a concern, a series resistance could have been connected with the capacitor, or SCRs (Silicon Controlled Rectifiers) could have been used for

switching. The pre- and post- disturbance waveforms were then analyzed by using the FFT (Fast Fourier Transform) in order to obtain the respective harmonic phasors.

3.3.2 Impedance calculation for single-phase three-wire systems

Figure 3-6 shows (a) the voltage source and (b) the current source equivalent circuit model for three-wire one-phase supply systems.

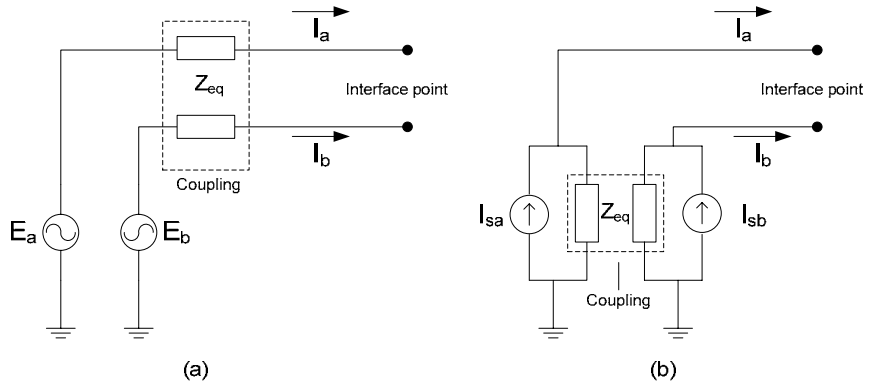

Figure 3-6 Equivalent circuit model: (a) Voltage source and (b) Current source.

The circuit equation is as follows:

$$\begin{bmatrix} V_a \\ V_b \end{bmatrix} = \begin{bmatrix} E_a \\ E_b \end{bmatrix} - \begin{bmatrix} Z_s & Z_m \\ Z_m & Z_s \end{bmatrix} \begin{bmatrix} I_a \\ I_b \end{bmatrix}, \tag{3-2}$$

where *Va*, *Vb*, *Ia* and *Ib* are the voltages and currents per branch, which can be measured at the interface point; *Zs* and *Zm* are the self-impedance and mutual impedance components of the equivalent network impedance *Zeq*. This circuit can be analyzed by using the Clarke transformation [22] as follows:

$$V_0 = \frac{1}{\sqrt{2}}(V_a + V_b) \quad V_\alpha = \frac{1}{\sqrt{2}}(V_a - V_b) \tag{3-3}$$

$$I_0 = \frac{1}{\sqrt{2}}(I_a + I_b) \quad I_\alpha = \frac{1}{\sqrt{2}}(I_a - I_b), \tag{3-4}$$

where subscripts 0 and α denote zero and the alpha sequence components. The impedance matrix after the transformation is

$$[Z_{0\alpha}] = [T][Z_{ab}][T]^{-1} = \begin{bmatrix} Z_s + Z_m & 0 \\ 0 & Z_s - Z_m \end{bmatrix}.$$

In other words, zero and alpha impedance components are $Z_0 = Z_s + Z_m$ and $Z_\alpha = Z_s - Z_m$, respectively. Equation (3-1) can be now applied as follows:

$$Z_{(\alpha,0)h} = -\frac{\Delta V_{(\alpha,0)}}{\Delta I_{(\alpha,0)}} = -\frac{V_{(\alpha,0)pre(h)} - V_{(\alpha,0)post(h)}}{I_{(\alpha,0)pre(h)} - I_{(\alpha,0)post(h)}}. \tag{3-5}$$

The self and mutual components are obtained by applying the inverse transformation:

$$Z_{(s)h} = \frac{Z_{(0)h} + Z_{(\alpha)h}}{2} \tag{3-6}$$

$$Z_{(m)h} = \frac{Z_{(0)h} - Z_{(\alpha)h}}{2}. \tag{3-7}$$

In summary, the supply harmonic impedances can be determined by using the following procedure:

- Input data. Collect the voltage and current waveforms. These data must contain the pre- and post-disturbance cycles. Select one pre- and one post-disturbance cycle.
- Calculate the fundamental and harmonic spectra for voltages and current by using DFT or FFT.

- Determine α and 0 components for V and I.
- Compute network harmonic impedance by using (3-5).
- Apply inverse transformation to obtain the self and mutual impedances.

3.3.3 Implementation issues

In power systems, the nominal frequency is 50 or 60 Hz. However, the operating frequency can vary by ± 0.1% of the nominal frequency. The variation will cause a phase shift between the pre-disturbance and the post-disturbance samples, leading to an incorrect impedance estimate. A small phase shift at the fundamental frequency can cause significant errors at the harmonic frequencies. Although reference [21] has demonstrated the importance of phase shift correction, this study does not propose a method to determine the phase shift amount. After investigating several alternatives, we found that a simple FFT-based method can be used for the automatic determination of the phase shift amount. The method is summarized below:

- Select two different cycles of the pre-disturbance voltage waveform.
- Calculate the fundamental frequency angle for the selected cycles by using the FFT.
- Determine the phase shift by:

$$\theta = \frac{[\alpha_1 - \alpha_2]}{cyc_1 - cyc_2}$$

where cyc1 and cyc2 are the two pre-disturbance selected cycles, and α1 and α2 are the corresponding angles.

The voltage waveforms are used for the FFT analysis since the voltage is less distorted than the current. The pre-disturbance cycles will be used since the post-disturbance cycles contain transient components and they can corrupt the results.

Cyc1 and cyc2 should be as far apart as possible for improved accuracy. Furthermore, the average between the two branches should be calculated. Once the phase-shift amount is determined, the effect of frequency variation can be compensated by using the following equations:

$$V_{(0,\alpha)post-new} = V_{(0,\alpha)post-actual} \cdot e^{jh\theta n} \tag{3-8}$$

$$I_{(0,\alpha)post-new} = I_{(0,\alpha)post-actual} \cdot e^{jh\theta n}, \tag{3-9}$$

where n represents the total number of cycles between the pre- and post-disturbance selected cycles, θ is the phase shift, and h is the harmonic order. The phase correction is done over the transformed zero and alpha waveforms.

3.4 Simulation studies on the proposed scheme

The proposed method is first verified by using computer simulations. A test example is presented in the circuit in Figure 3-7. The circuit has a utility harmonic source with a medium phase voltage of 14.4kV for the fundamental frequency and third, fifth, seventh, ninth and eleventh harmonic components, each one with a magnitude of 1% of the nominal fundamental voltage. The primary system impedance is (1.0004+j3.7699)Ω. The distribution transformer is a 10kVA single-phase transformer 14.4kV/240V with 2% impedance. The secondary conductor is a 4/0 Triplex, 4/0 ACSR neutral with 50m of length. Mutual effect is also considered. A 1200 μF capacitor is switched on at 80 ms (within the fifth cycle of the simulation). The system was set up intentionally at 59.8 Hz to produce a phase-shift effect. For this case, we have 1.20 degrees per cycle of phase shift due to frequency variation. This problem is overcome by using the procedure described in the previous section.

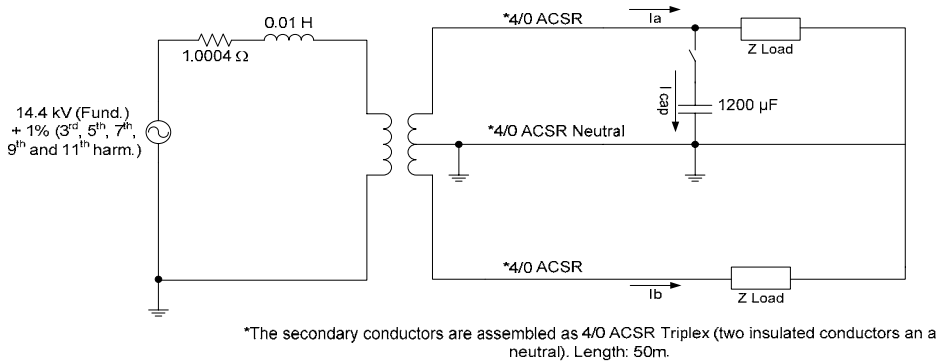

Figure 3-7 Test simulated circuit for example application.

Table 3-1 shows the self and mutual impedance values estimated by using the proposed method. Figure 3-8 presents them graphically (only the self impedances). The results are further compared with the actual model data. Phase-shift correction was considered and Table 3-1 shows a good agreement among the results.

Table 3-1 Harmonic impedance results.

	Actual value [Ω]		Proposed method [Ω]	
	Self	Mutual	Self	Mutual
R_1	0.027	0.000	0.026	0.000
X_1	0.033	-0.022	0.034	-0.023
R_3	0.027	0.000	0.027	-0.001
X_3	0.099	-0.065	0.100	-0.066
R_5	0.027	0.000	0.027	-0.001
X_5	0.165	-0.108	0.167	-0.110
R_7	0.027	0.000	0.026	0.001
X_7	0.231	-0.152	0.233	-0.154
R_9	0.027	0.000	0.027	0.000
X_9	0.297	-0.195	0.300	-0.198
R_{11}	0.027	0.000	0.028	-0.001
X_{11}	0.364	-0.239	0.369	-0.244

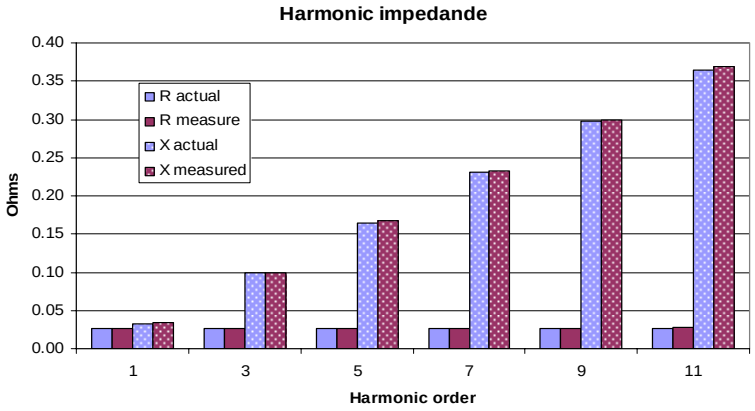

Figure 3-8 Harmonic results for test simulated circuit.

3.5 Experimental results

The proposed method's performance was further evaluated through field measurements. A residential site with a known supply system data was used for this purpose. Figure 3-9 shows the experimental set-up. The capacitor bank was switched about 50 times to yield 50 sets of results. It was used the same rejection threshold as reference [21]: $(\Delta I_h / \Delta I_1) < 1\%$. The test's duration is about 15 minutes excluding the set-up and dismantling. It is therefore reasonable to assume that no significant system side change occurred during such a short period.

All voltage and current signals at the metering point were recorded. For each signal, 15 cycles were taken, which consisted of 4 pre-disturbance cycles and 10 post-disturbance cycles (see Figure 3-5). The disturbance (switching the capacitor to "on") occurred at the fifth cycle. The sample rate was 256 points per cycle.

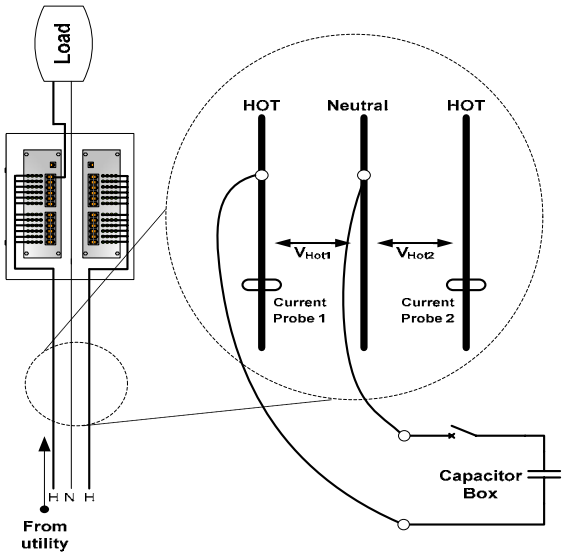

Figure 3-9. System set-up used in field measurements.

Figure 3-10 shows the key results of the proposed method, the changes in the voltage and current, and the resulting impedance values. There is a good consistency among the switching events or cases.

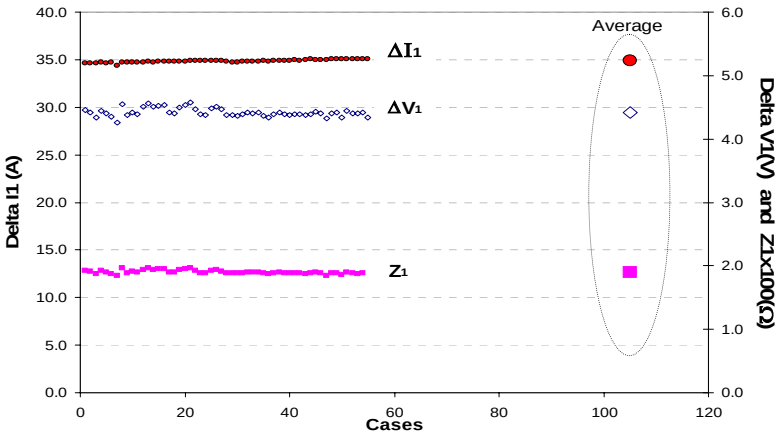

Figure 3-10 Field measurement results.

For the test site, the supply system data such as the size of the transformer and the type and length of the secondary conductors are known. Therefore, the field results can be compared with those calculated from component models. Table 3-2 shows the comparison and reveals that the agreement is good. Although the component model data have some uncertainties, the results confirm that the proposed measurement method is adequate.

Table 3-2 Calculated and Measured Impedance

		$R_1[\Omega]$	$X_1[\Omega]$
Z_{self}	Calculated	0.0988	0.0450
	Measured	0.1093	0.0660
Z_{mutual}	Calculated	0.0494	0.0225
	Measured	0.0552	0.0277

Figure 3-11 shows the scatter plots (R-X) for the harmonic impedances. The 9th harmonic data are slightly spread due to this harmonic's low voltage change level. Figure 3-12 shows the trends of the self and mutual harmonic components R*(h)* and X*(h)*. Self harmonic resistances have a roughly constant value for each harmonic order. On the other hand, the harmonic reactances increase linearly with the frequency. No resonance is observed. From the 50-plus test results, a more accurate impedance value was estimated by using least square fitting of the results (see Figure 3-12). The fitting equations were determined as

$$\begin{aligned} R_s(h) &= (-0.0012h + 0.1093)\Omega \approx 0.1093\Omega \\ R_m(h) &= (0.0005h + 0.0552)\Omega \approx 0.0552\Omega \\ X_s(h) &= (0.0660h + 0.0017)\Omega \approx (0.0660h)\Omega \\ X_m(h) &= (0.0277h + 0.0031)\Omega \approx (0.0277h)\Omega \end{aligned} .$$

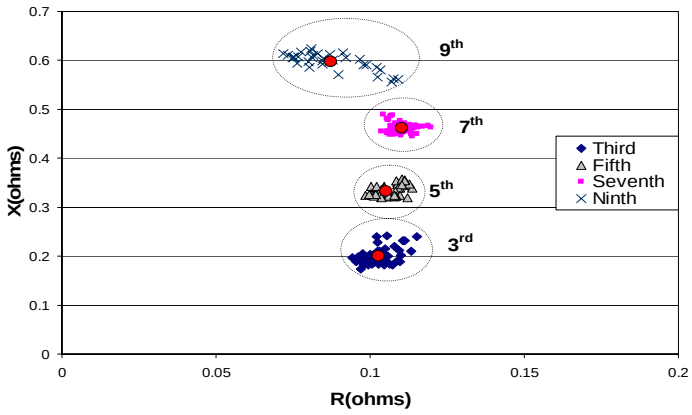

Figure 3-11 Harmonic impedance results. Scatter plot for harmonic orders.

As a result, we can conclude that the system impedance values are R_s=0.1093**Ω**, X_s=0.0660**Ω** and R_m=0.0552**Ω**, X_m=0.0277**Ω** at 60Hz.

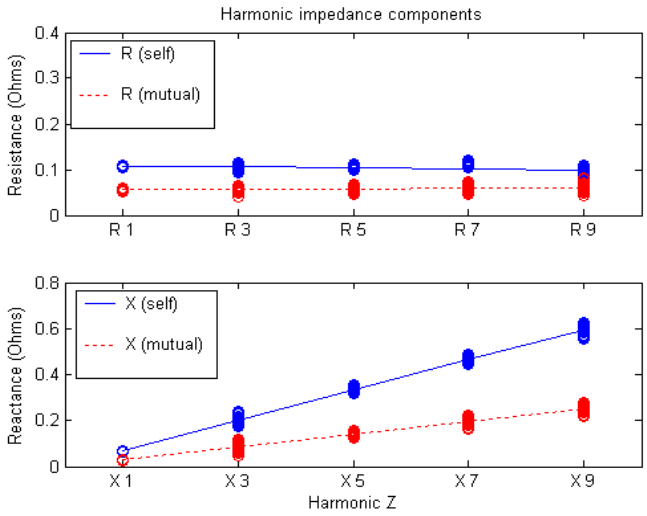

Figure 3-12 Harmonic impedance trends.

The above results have shown that the proposed technique is a practical and reliable method to determine the harmonic impedances of single-phase three-wire supply systems. The method uses a simple portable capacitor bank to create sufficient waveform changes for impedance determination. It relies on steady-state

waveforms for impedance determination. As a result, a high sampling rate is not necessary. Most common power quality monitors can be used to implement the method, which has been tested by using simulation studies and field measurements.

3.6 Potential application – Harmonic source determination

One strategy of harmonic management interested by utilities is to measure the harmonic emission levels from a customer at the utility-customer interface point [10]-[11]. The results will reveal how many harmonic currents are actually produced by a customer and what is the impact of background harmonics in the utility supply system.

Unfortunately, field measurement of harmonic contributions due to a customer and its supply system is not a trivial task. One must determine the harmonic sources contained in both customer and utility systems first. Only after obtaining the source information, can each side's contribution to the harmonic current measured at the interface point be determined. Several papers have proposed methods to solve the problem [23-34]. However, all methods are developed for three-phase systems and assuming balanced system conditions. They are not readily applicable to measure harmonic sources in three-wire single-phase systems.

In response to industry's interest in determining harmonic sources and harmonic contributions at the utilization voltage levels, we have been researching a practical and systematic harmonic source measurement technique. The current source equivalent supply system seen from the interface point was presented in Figure 3-1. Once the harmonic impedance results are available, it becomes possible to calculate the Thevenin or Norton sources in 0-α domain (as shown in section 3.3.2) and then in phase domain. The equations are:

$$V_{(\alpha,0)h} = E_{(\alpha,0)h} - Z_{(\alpha,0)h} I_{(\alpha,0)h} \tag{3-10a}$$

$$I_{(\alpha,0)h} = I_{S(\alpha,0)h} - \frac{V_{(\alpha,0)h}}{Z_{(\alpha,0)h}} \tag{3-11b}$$

In phase quantities:

$$E_{(a)h} = \frac{\sqrt{2}}{2}\left(E_{(0)h} + E_{(\alpha)h}\right), \quad E_{(b)h} = \frac{\sqrt{2}}{2}\left(E_{(0)h} - E_{(\alpha)h}\right) \tag{3-12a}$$

I_s per phase follows the same pattern as E_a and E_b. All analyses have been developed assuming that the power flows from the utility to customer. This assumption is needed in order to be consistent with the model and to obtain meaningful results.

Figure 3-14 presents the voltage and current waveforms measured at the site without the capacitor bank. Significant harmonic distortions can be seen in both waveforms without the help of spectrum analysis. In fact, the waveforms are representative of the various sites we have measured in the past. They are vivid illustrations of the harmonic problems prevalent at the utilization voltage levels.

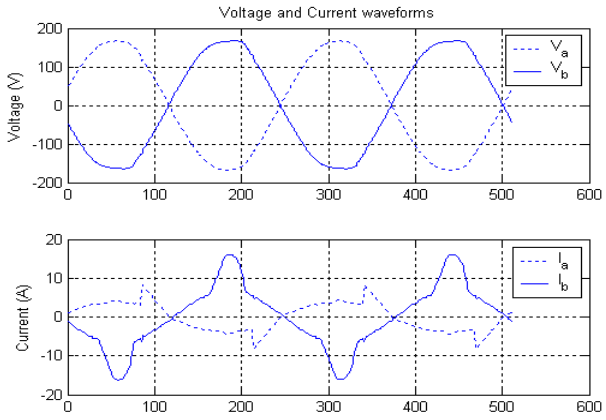

Figure 3-13 Detail of voltage and current waveforms per phase (2 cycles).

Using the proposed technique, the harmonic sources of the supply system are determined. Table 3-3 summarizes the results for the site, which includes the magnitudes of the harmonic current sources in the supply system and those at the metering point. The results confirm that the system does contain harmonic sources (I_{sa} and I_{sb}). The harmonic source magnitudes are less than 1.5% of its fundamental frequency value. However, they are quite large in comparison with the harmonic currents actually flowing at the metering point (I_a and I_b). This observation seems to suggest that the small system impedance may have bypassed most of the harmonic source currents that would flow to the customer side otherwise. At this stage, it is not possible to determine how much current actually penetrates to the customer side since the customer impedance is unknown. How to determine the impedance at the customer side is presented in next chapter.

Table 3-3 Harmonic source results and harmonic phase currents

h	I_{sa} [A]	I_a [A]	I_{sb} [A]	I_b [A]
1	1874.3∠-109.8	3.44∠88	1872.0∠70.1	7.59∠-100
3	20.69∠-39.7	0.83∠32.2	26.77∠136.2	2.23∠63.1
5	8.97∠126.4	0.59∠-56.1	12.67∠-57.1	1.43∠-132.5
7	4.79∠-58.8	0.40∠-170.1	5.59∠122.5	0.62∠32.4
9	2.31∠66.7	0.23∠53.8	2.41∠-114.8	0.11∠-115.8

3.7 Conclusions and major findings

Harmonic impedance is an important parameter in power system analysis and must be known to characterize frequency responses and harmonic propagations in a power network. The research presented in this chapter has resulted in a practical and reliable method for determining the harmonic impedances of single-phase three-wire supply systems. The main conclusions and contributions of this chapter are summarized as follows:

- The method uses a simple portable capacitor bank to create sufficient waveform changes for impedance determination. Results show that a capacitor size around 1mF is sufficient for measuring most residential customers.

- The method uses steady-state waveforms for impedance determination. As a result, high sampling rate is avoided. Most common power quality monitors can be used to implement the method.

- The proposed method has been tested using simulation studies and field measurements. Its performance and accuracy have been found very good. The method is adequate for determining the harmonic impedances and sources contained in the supply system.

In summary, the supply harmonic impedances and harmonic sources can be determined using the following procedure:

1. Input data. Collect the voltage and current waveforms. This data must contain pre- and post-disturbance cycles. Select one pre- and one post-disturbance cycle.
2. Calculation of fundamental power and harmonic spectra for voltages and current using DFT or FFT.
3. Determine α and 0 components for *V* and *I* using (3-3) and (3-4).
4. Correct phase shift according to Section 3.3.3.
5. Compute network harmonic impedance using (3-5). Reject the values below the threshold $\left(\Delta I_h / \Delta I_1\right) < 1\%$.
6. Calculate harmonic sources using (3-10).
7. Apply inverse transformation to obtain self and mutual impedances and harmonic sources.

Chapter 4

Customer-side harmonic impedance

Developing an accurate representation of composite loads is a challenging task because they are often composed of many devices such as lighting, appliances, heaters, motors, computers and furnaces; therefore, precise information on the exact composition of a load is frequently lacking. Furthermore, new load components alter system characteristics, and currently, no accurate tests are available for verifying load models.

As previous chapters indicate, extensive research has been carried out to provide system impedance results. Although customer-side impedance determination follows similar procedures, several practical issues make this estimation more difficult: (1) loads vary with time more frequently than their system-side counterparts do; (2) most of the disturbance transients travel to the system side instead of the load side; and (3) the loads are less susceptible to voltage change due to capacitor switching.

In this chapter, a measurement-based approach is presented to estimate the load parameters for fundamental and harmonic components. The proposed approach was tested through simulations and field measurement tests. The field measurement results were processed to estimate the impedances of the load sides by using the same set of data used for the system side. In Section 4.1, the impedance measurement scheme is presented and applied to the proposed load model, which is presented in Section 4.2. Implementation issues are discussed in Section 4.3. Finally, major findings are presented in Section 4.4.

4.1 Impedance measurement methodology

A methodology to estimate harmonic impedances at the load side of the Point of Common Coupling (PCC) for single-phase systems served at 120V/208V is presented here. The method to calculate load-side impedance is very similar to that utilized for system-side impedance. In this case, the current ($I_{load\text{-}side}$) downstream from the capacitor was used, as shown in Figure 4-1. In a general sense, load impedance can be calculated by the ratio

$$Z_{load} = \frac{\Delta V}{\Delta I_{load\ side}}, \tag{4-1}$$

where ΔV and $\Delta I_{load\text{-}side}$ represent the subtraction of the voltage and the currents, respectively, before and after the capacitor switching. The details about the fundamental and harmonic load impedance calculations are presented in Section 4.2. In practical cases, only the system and capacitor currents can be measured; as a result, the load site current is calculated from the measured system and capacitor currents:

$$I_{load\ side} = I_{system\ side} - I_{cap}. \tag{4-2}$$

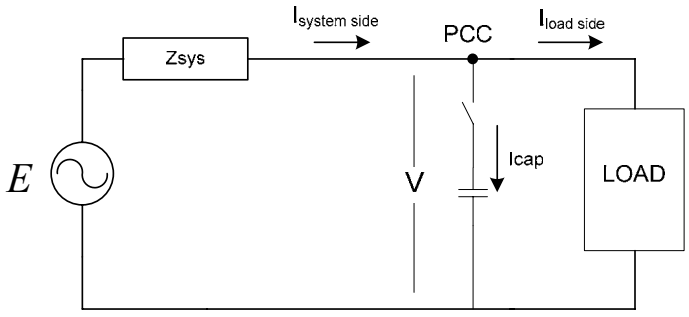

Figure 4-1 Load-side impedance measurement approach.

4.2 Equivalent model for single-phase systems

Although the above impedance measurement technique is simple in theory, its application to the loads is a challenging task, since not all measurements of the current are available to directly estimate the impedances. A single-phase load always involves two branches as shown in Figure 4-2. In practical cases, voltage and current measurements are available only at each branch, so that only the phase currents Ia_{pcc} and Ib_{pcc} can be accessed, but not the currents flowing through the impedances Z_1, Z_2 and Z_3, which are not available to be measured. This problem increases the complexity of estimating customer-side load impedances.

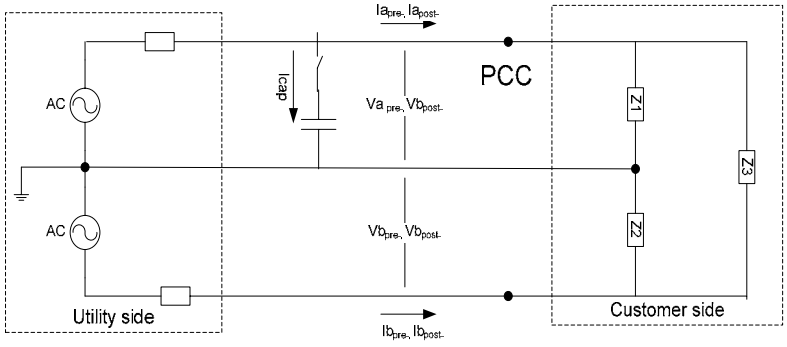

Figure 4-2 Typical single-phase supply with two branches.

In order to overcome this difficulty, a new equivalent model for the two-branch load has been developed and is presented in Figure 4-3. The load impedances for this system can be represented by two equivalent phase-to-neutral impedances, Z_{a_eq} and Z_{b_eq}, which are the parallel of half of the phase-to-phase impedance Z_3 with each original phase impedance (Z_1, Z_2), respectively. In this way, the impedance estimation is performed for the two branches simultaneously. The results are two equivalent impedances, Z_{a_eq} and Z_{b_eq}. The results are two equivalent impedances, Z_{a_eq} and Z_{b_eq}. Equation (4.3) represents the impedance estimation:

$$Z_{a\_eq} = Z_1 \| \left(Z_3 / 2 \right) \cdot \qquad (4\text{-}3)$$
$$Z_{b\_eq} = Z_2 \| \left(Z_3 / 2 \right)$$

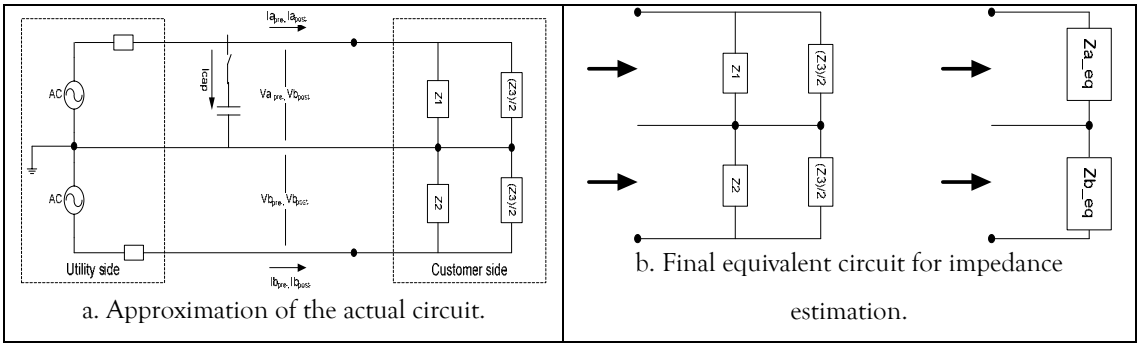

a. Approximation of the actual circuit.

b. Final equivalent circuit for impedance estimation.

Figure 4-3 Equivalent proposed model for a single-phase two- branch system.

For fundamental components, equivalent impedances can be determined be using either the ratio *V/I* or ΔV/ΔI, which is obtained from a capacitor switching. This *ΔV/ΔI* ratio is also used to estimate the impedance for harmonic orders, as is shown in equation (4-4):

$$Za_{eq-h} = \frac{Va_{pcc\_h-post} - Va_{pcc\_h-pre}}{Ia_{pcc\_h-post} - Ia_{pcc\_h-pre}} = \frac{\Delta V_h}{\Delta I_h}, \qquad (4\text{-}4)$$

where V_{pre} and I_{pre} represent the voltage and current phasors before the capacitor is switched; conversely, V_{post} and I_{post} are obtained after the switching. The subscript *h* represents the harmonic order. The branch *b* impedance, Z_{b_eq}, is similarly calculated.

4.2.1 Simulation results

The circuit presented in Figure 4-4 was simulated. The supply system was represented by two voltage sources of 120V per branch, which were connected to the load side through branch impedances of $(0.062+j0.03)\Omega$. The load side was composed of the impedances Z_1= $(1.18+j0.754)\Omega$, $Z2$= $(0.73+j1.508)\Omega$ and Z_3= $(5.0+j1.885)\Omega$. Fifth-order harmonic sources were intentionally added at each load in order to have some harmonic background. 5.5A were injected into each branch and another source of 10A was connected in parallel with Z_3.

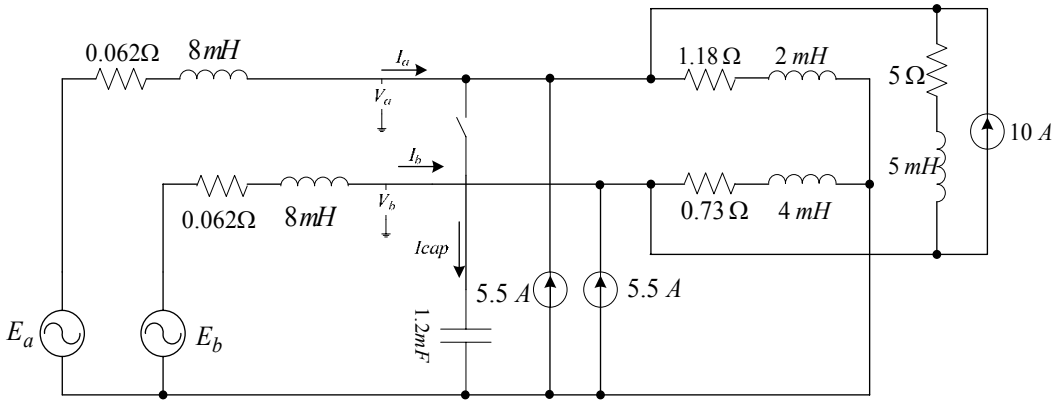

Figure 4-4 Single-phase simulation case.

A 1200 μF was switched after the fifth cycle of the simulation. In Figures 4-5 and 4-6, the recorded waveform and the harmonic spectra of the voltage and currents of each branch are presented. As expected, only the fundamental and fifth harmonic components are present. Table 4-1 shows the equivalent impedance results obtained for these frequency components. These results agree closely with the expected values.

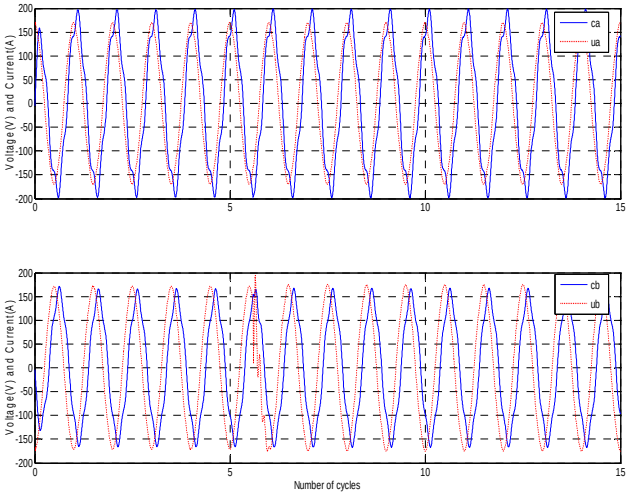

Figure 4-5 Branch currents and voltage waveforms.

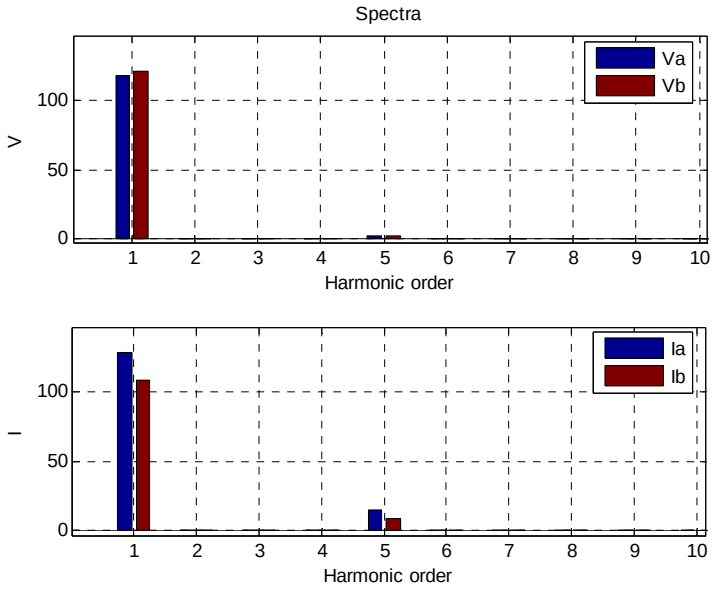

Figure 4-6 Branch currents and voltage harmonic spectra.

Table 4-1 Simulation load impedance results

	Fundamental		5th harmonic	
	Za_eq[Ω]	Zb_eq[Ω]	Za_eq[Ω]	Zb_eq[Ω]
Expected	**0.8115+j0.4403**	**0.7439+j0.8158**	**0.8491+j2.1150**	**1.0229+j3.0206**
PSCAD® simulation	0.8156+j0.4343	0.7473+j0.8217	0.8556+j2.1448	1.0265+j3.0219

4.2.2 Field measurement results for fundamental frequency

A sample site was selected to evaluate the impedance results. This site was a commercial customer (a small convenience store), where 30 snapshots were taken (15 switching events for each branch). The fundamental impedance was calculated by using three methods: V_{pre}/I_{pre}, V_{post}/I_{post} and $\Delta V/\Delta I$. Figure 4-7 shows the results obtained for this particular site. The results of the V/I approaches (presented in table 4.2) are almost identical and consistent. In general, the $\Delta V/\Delta I$ approach agrees for the snapshots where the capacitor was switched on (see Figure 4-7), because the energy level on the switched branch was much higher than on the non-switched one.

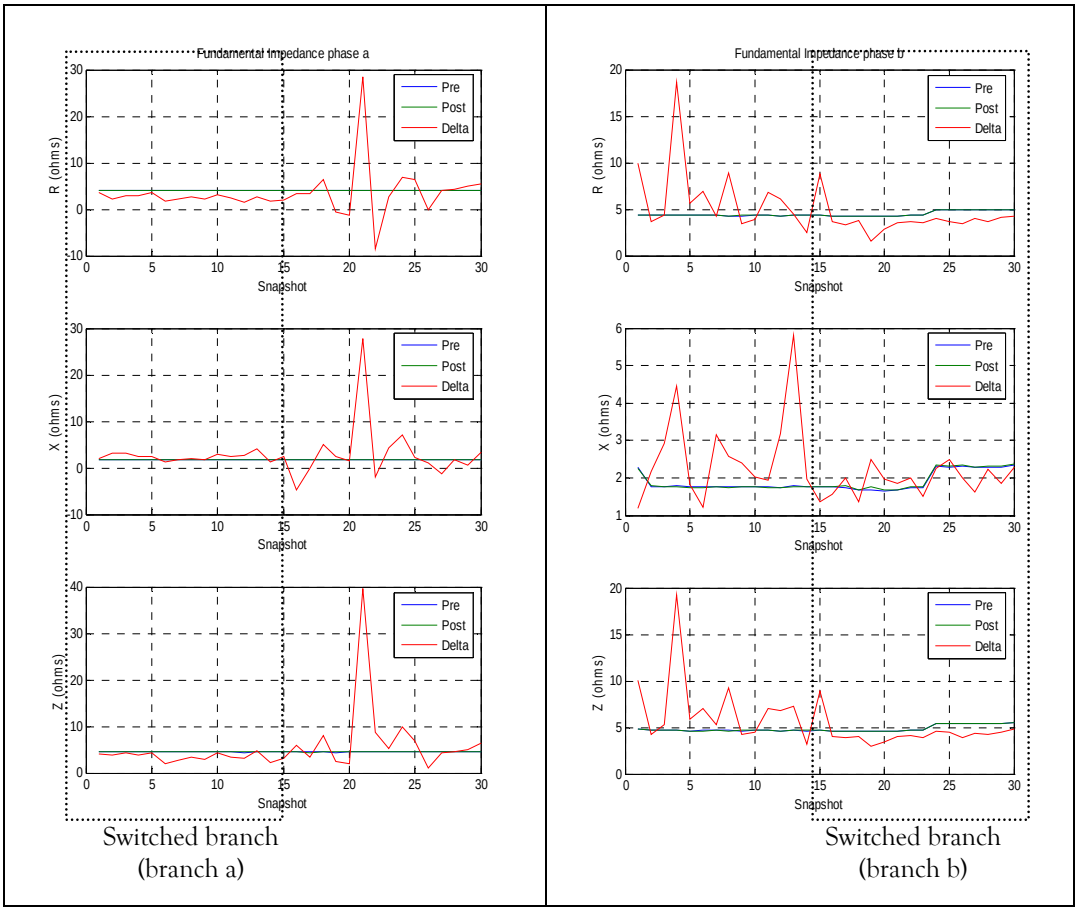

Figure 4-7 Fundamental impedance. Comparison using V/I and ΔV/ΔI.

Since each measured field case included multiple snapshots, multiple estimated impedance values were obtained. Figure 4-8 presents the scatter plots, which show consistent results for the fundamental component for the analyzed site. As expected, the estimated load impedances are much more scattered among the various snapshots, mainly due to the energy level available for load-side impedance determination, as explained in Section 4.3. Because the system side had much smaller impedances, most of the capacitor-switching transients traveled to the system side instead of the load side. Thus, the determination of load impedance was much more challenging and fewer snapshots yielded acceptable results. Therefore, the estimated load impedances are less reliable than the estimated system impedances.

Table 4-2: Numerical results for fundamental load impedance.

	Vpre/Ipre		*Vpost/Ipost*		*ΔV/ΔI*	
Snapshot	*Za_eq*[Ω]	*Zb_eq*[Ω]	*Za_eq*[Ω]	*Zb_eq*[Ω]	*Za_eq*[Ω]	*Zb_eq*[Ω]
1	4.098 + 1.735i	4.311 + 2.294i	4.100 + 1.747i	4.308 + 2.255i	**3.656 + 1.954i**	9.977 + 1.185i
2	4.088 + 1.768i	4.307 + 1.774i	4.140 + 1.820i	4.317 + 1.782i	**2.105 + 3.160i**	3.686 + 2.176i
3	4.081+ 1.744i	4.314 + 1.772i	4.115 + 1.775i	4.325 + 1.766i	**2.807 + 3.201i**	4.403 + 2.918i
4	4.092 + 1.773i	4.317 + 1.794i	4.098 + 1.802i	4.314 + 1.766i	**2.895 + 2.394i**	18.72 + 4.451i
5	4.086 + 1.751i	4.304 + 1.761i	4.102 + 1.770i	4.302 + 1.743i	**3.549 + 2.422i**	5.634 + 1.824i
6	4.112 + 1.696i	4.310 + 1.760i	4.064 + 1.803i	4.305 + 1.738i	**1.670 + 1.242i**	6.944 + 1.215i
7	4.120 + 1.711i	4.312 + 1.771i	4.104 + 1.783i	4.327 + 1.764i	**2.174 + 1.668i**	4.190 + 3.161i
8	4.088 + 1.718i	4.299 + 1.777i	4.091 + 1.766i	4.300 + 1.746i	**2.595 + 2.087i**	8.862 + 2.586i
9	4.094 + 1.687i	4.297 + 1.770i	4.084 + 1.758i	4.311 + 1.777i	**2.179 + 1.746i**	3.468 + 2.403i
10	4.073 + 1.743i	4.305 + 1.771i	4.103 + 1.771i	4.312 + 1.776i	**3.133 + 2.841i**	3.935 + 2.031i
11	4.075 + 1.718i	4.314 + 1.772i	4.095 + 1.770i	4.312 + 1.746i	**2.500 + 2.411i**	6.794 + 1.950i
12	4.059 + 1.714i	4.293 + 1.747i	4.106 + 1.788i	4.300 + 1.726i	**1.618 + 2.681i**	6.076 + 3.180i
13	4.075 + 1.740i	4.316 + 1.783i	4.115 + 1.763i	4.330 + 1.765i	**2.690 + 4.069i**	4.453 + 5.800i
14	4.126 + 1.737i	4.305 + 1.753i	4.084 + 1.813i	4.321 + 1.770i	**1.737 + 1.324i**	2.492 + 1.973i
15	4.108 + 1.727i	4.311 + 1.778i	4.118 + 1.783i	4.306 + 1.760i	**2.036 + 2.377i**	8.763 + 1.349i
16	4.128 + 1.747i	4.302 + 1.756i	4.106 + 1.733i	4.292 + 1.767i	3.483 - 4.683i	**3.655 + 1.576i**
17	4.111 + 1.705i	4.292 + 1.746i	4.072 + 1.710i	4.294 + 1.783i	3.488 - 0.028i	**3.293 + 2.006i**
18	4.095 + 1.690i	4.285 + 1.682i	4.108 + 1.666i	4.269 + 1.692i	6.390 + 4.953i	**3.756 + 1.359i**
19	4.076 + 1.704i	4.269 + 1.678i	4.110 + 1.678i	4.295 + 1.752i	-0.480 + 2.417i	**1.618 + 2.497i**
20	4.095 + 1.742i	4.263 + 1.650i	4.126 + 1.693i	4.259 + 1.685i	-1.313 + 1.548i	**2.816 + 1.964i**
21	4.116 + 1.726i	4.267 + 1.670i	4.116 + 1.696i	4.265 + 1.687i	28.46 + 27.71i	**3.580 + 1.846i**
22	4.117 + 1.751i	4.403 + 1.746i	4.115 + 1.697i	4.402 + 1.764i	-8.418 - 2.041i	**3.656 + 1.990i**
23	4.100 + 1.731i	4.405 + 1.732i	4.129 + 1.719i	4.390 + 1.754i	2.772 + 4.316i	**3.571 + 1.517i**
24	4.100 + 1.750i	4.946 + 2.311i	4.112 + 1.721i	4.936 + 2.335i	6.826 + 7.102i	**4.053 + 2.245i**
25	4.106 + 1.705i	4.924 + 2.283i	4.106 + 1.687i	4.921 + 2.322i	6.481 + 2.238i	**3.660 + 2.496i**
26	4.094 + 1.735i	4.942 + 2.306i	4.135 + 1.689i	4.919 + 2.331i	-0.197 + 1.126i	**3.413 + 1.993i**
27	4.123 + 1.717i	4.944 + 2.280i	4.093 + 1.703i	4.914 + 2.294i	4.163 - 1.387i	**4.052 + 1.618i**
28	4.085 + 1.688i	4.945 + 2.281i	4.086 + 1.686i	4.931 + 2.321i	4.243 + 1.849i	**3.609 + 2.224i**
29	4.130 + 1.705i	4.949 + 2.285i	4.118 + 1.696i	4.927 + 2.303i	4.951 + 0.537i	**4.097 + 1.858i**
30	4.081 + 1.725i	4.956 + 2.347i	4.099 + 1.697i	4.948 + 2.376i	5.395 + 3.329i	**4.214 + 2.300i**

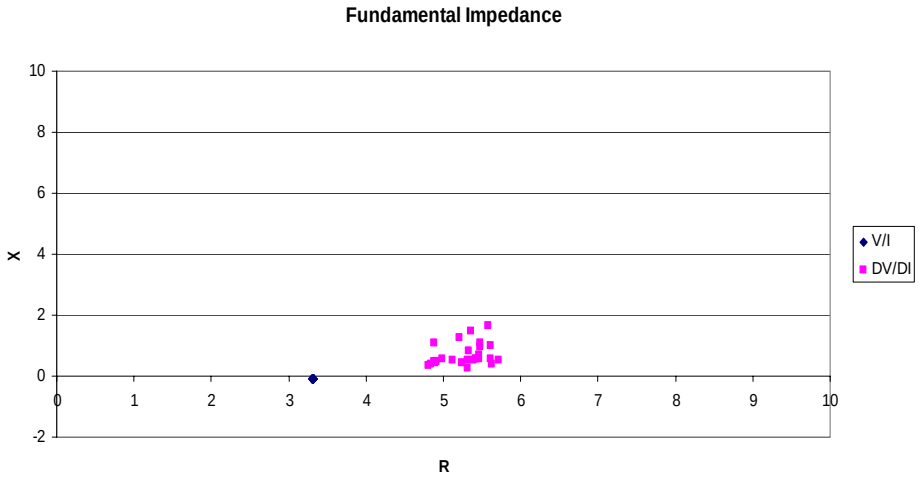

Figure 4-8 Fundamental component results for measured load impedance.

4.2.3 Harmonic load impedance

Figure 4-9 presents the impedance data obtained from one of the measured sites. All harmonic orders have consistent results. Table 4-3 presents the sample results for other of sample sites tested. The blank spaces in the table indicate values that could not be determined due to low energy levels, scattered out points or negative values or resistance. The load impedance results for other measured sites are presented in Chapter 6.

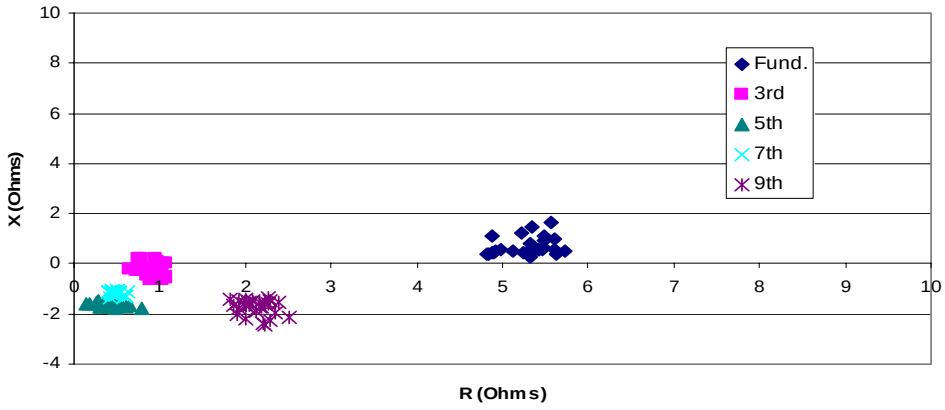

Figure 4-9 Sample measured load impedances.

Table 4-3 Load impedance results for some sample sites

Branch a														
Site	**R_1**	**R_3**	**R_5**	**R_7**	**R_9**	**R_{11}**	**R_{13}**	**X_1**	**X_3**	**X_5**	**X_7**	**X_9**	**X_{11}**	**X_{13}**
2	12.312	1.749	1.586	0.405	3.283	0.393	1.746	4.018	-0.775	0.778	0.073	0.815	-0.073	2.465
3	5.184	0.915	0.426	0.486	2.119	0.962	4.780	0.688	-0.174					1.658
13	16.994		3.305	2.605	1.197	0.282	0.306	-3.614		4.895	0.356	-0.714		-0.399
15	13.815	8.401	18.106	8.050	2.582	0.976	0.957	4.726	3.269	-0.965	0.001	-1.626	0.084	0.804
Branch b														
Site	**R_1**	**R_3**	**R_5**	**R_7**	**R_9**	**R_{11}**	**R_{13}**	**X_1**	**X_3**	**X_5**	**X_7**	**X_9**	**X_{11}**	**X_{13}**
2	10.964	2.542	2.945	1.047	2.901	0.189	0.119	2.577	-0.034	2.150	-0.200	0.611	0.230	1.504
3	5.077	1.485		1.103		0.803		0.691	-1.343					
13	26.796		10.841	3.905	4.493	1.040	0.977	2.233		20.594	1.702			-2.106
15	13.455	3.307	5.356	3.156	0.387	0.555	0.251	0.961	-3.196	8.079	-0.328		-0.289	-0.053

4.3 Implementation issues

As mentioned at the beginning of this chapter, load impedance estimation faces in terms of practical and implementation issues. Network parameter uncertainty and load configuration may cause significant variations as shown in [35]. This section describes how energy levels, load variation and other issues play an important role in the estimation of the impedance results.

4.3.1 Energy level

Figures 4-10 and 4-11 show the spectra of voltage and current and their respective ΔV and ΔI for two different measured sites. The first site offers good and consistent results, whereas the second one has poor impedance results. The first site has higher values for ΔV and ΔI than those of the second site. Low energy levels, therefore, can be used to identify unreliable results. An extensive analysis of the reliability measurement is presented in the next chapter.

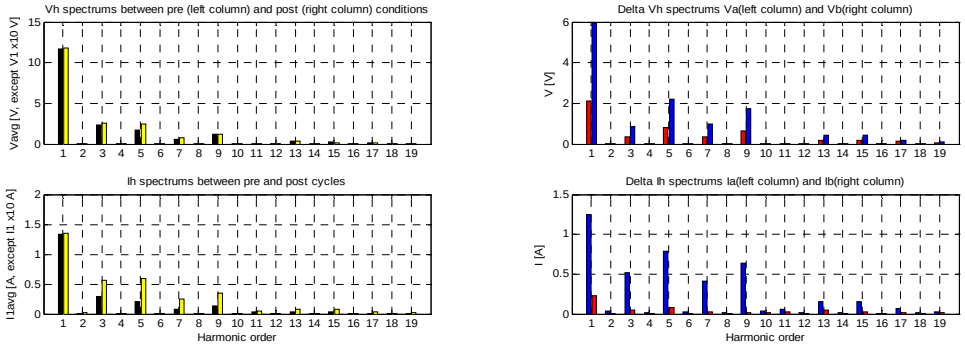

a. b.

Figure 4-10 Energy levels for a successful site. a. *V* and *I*; b. *ΔV* and *ΔI*.

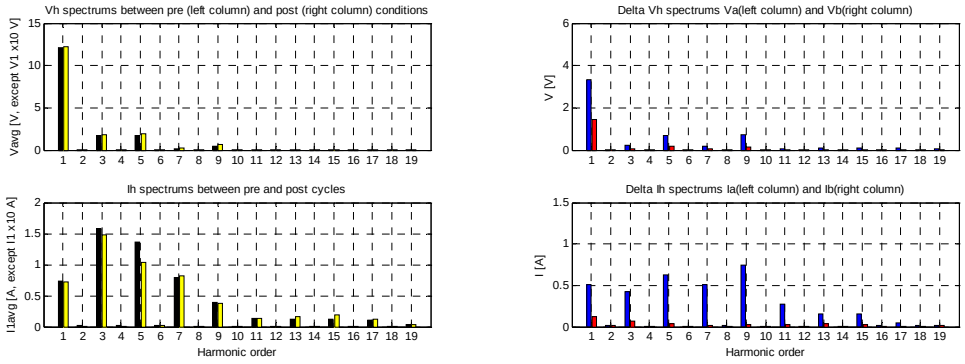

a. b.

Figure 4-11 Energy levels for an unsuccessful site. a. V and I; b. ΔV and ΔI.

4.3.2 Load variation

A typical load is composed of many devices. Each device or new component alters the load characteristics. In addition, loads vary with time and may include many continuous and discrete controls and protections. As a result, researchers need to ensure that no significant load changes occur between the pre- and post-disturbance measured data. Figure 4-12 shows the real and reactive power for each branch. In order to obtain consistent and reliable results, researches must ensure that either no variation or only slight variation occurs.

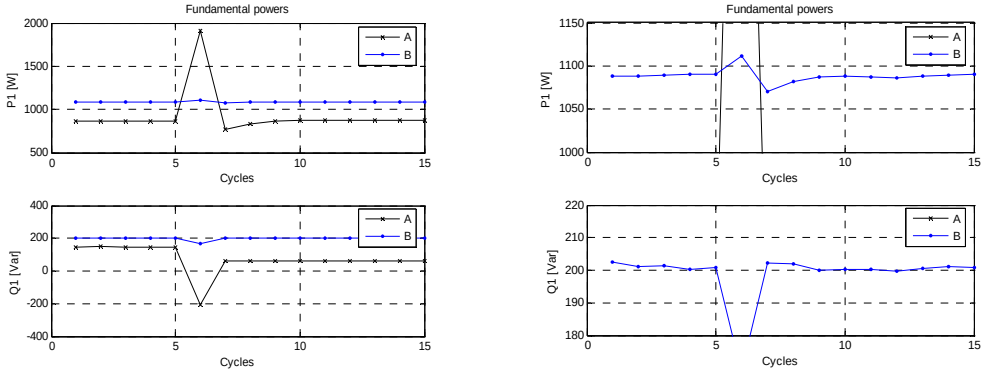

a. Active and reactive power. **b. Zoom in for branch b.**

Figure 4-12 Load variation.

4.3.3 Subtraction of waveforms

The branch currents used in load-side impedance calculations must be obtained by subtracting the capacitor current from the actual measured current at the utility side. This subtraction can propagate measurement errors and eventually affect the impedance calculation. The set of data used in this thesis was based on multi-channel measurements; therefore, all the channels had to be sampled synchronously. Due to hardware costs and constraints, however, a common data-acquisition practice is to sample the channels sequentially. Since the acquired signals (currents and voltages) are recorded sequentially, a time delay occurs that produces what is called a *skewing error*. Load impedance results are significantly sensitive to this time delay. Several ways to correct this error are discussed in the literature [36-37]. For instance, one way is to increase the number of points per cycle and then align the signals to be subtracted [38]. Depending on the number of points increased, this approach may be computationally inefficient. The method for skewing-error correction used here is based on the principle of linear interpolation. Assume that the first channel is the reference channel to which the values of all the other channels will be aligned; then, the corrected value of the 4th channel can be calculated according to Figure 4-13 and Equation (4-5):

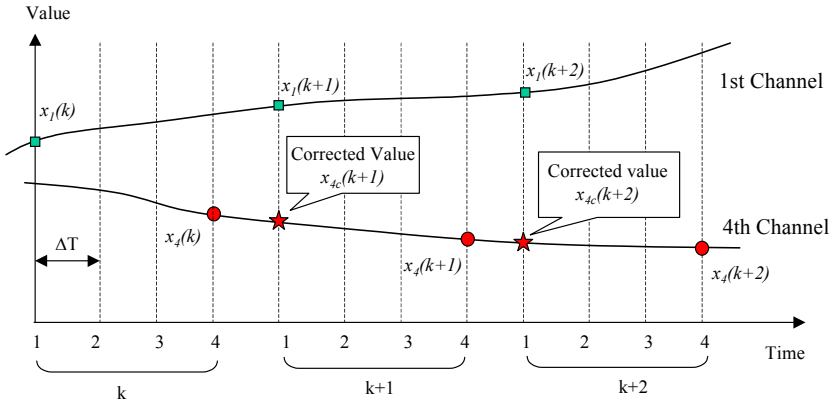

Figure 4-13 Correction of skewing error for the sequential interval sampling scheme.

$$x_{4c}(k+1) = \frac{x_4(k+1) - x_4(k)}{4\Delta T}(4\Delta T - 3\Delta T) + x_4(k) = \frac{3}{4}x_4(k) + \frac{1}{4}x_4(k+1), \tag{4-5}$$

where subscript *c* indicates the corrected value. Equation (4-5) shows that the corrected value is the weighted summation of two adjacent values. Since $x_4(k)$ is closer to the reference time, it has a weighting factor of 3/4. $x_4(k+1)$ is 3ΔT away from the reference time. Its weighting factor is 1/4. The general correction formula for the *N* channel sequential interval sampling scheme is

$$x_{nc}(k+1) = \frac{n-1}{N}x_n(k) + \frac{N-(n-1)}{N}x_n(k+1), \tag{4-6}$$

where *N* is the total number of channels, and *n* is the specific channel number. For the 1st channel, $n=1$ and $x_{1c}(k+1)=x_1(k+1)$, the corrected value equals the sampled value. Figure 4-14 shows how this error was corrected for the branch currents at each side of the interface point and the error generated by the subtraction of the capacitor current.

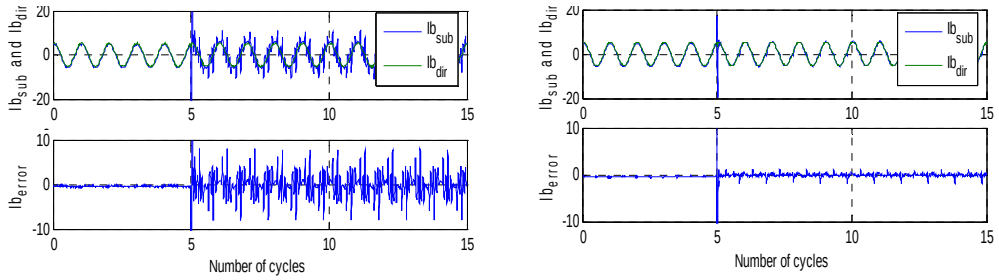

Before correction After correction

Figure 4-14 Subtraction error.

4.4 Summary and major findings

This chapter proposed a method to estimate the load-site impedances, and the results revealed some interesting characteristics of the loads from information that was relatively easy to obtain (the same set of data were utilized for system impedance estimation). The proposed approach relies on the load being time-invariant. Despite the uncertainties, measurement errors (from load variations and the subtraction of waveforms), and approximations to equivalent models, the results show that the proposed model is simple and able to capture with acceptable accuracy the load impedance within a reasonable range.

Since the energies of the disturbance available to determine the load site impedances were much smaller than those for system-side impedance determination, the load impedance results are much more scattered among the various snapshots and therefore less accurate. This result occurred because most of the capacitor-switching transients traveled to the system side (smaller impedance) instead of the load side. Detailed field measurements results are presented in Chapter 6.

The customer-side harmonic impedance procedure can be summarized as follows:

1. Input data. Collect the voltage and current waveforms. This data must contain pre- and post-disturbance cycles. Select one pre- and one post-disturbance cycle.
2. Select a channel as reference, e.g. Channel 1: *Va*. Correct skewing error according to Equation 4-6.
3. Calculation of $I_{loas\ side}$ from $I_{system\ side}$ and I_{cap} using (4-2).
4. Calculation of fundamental power and harmonic spectra for voltages and current using DFT or FFT.
5. Calculate Z_{a_eq} and Z_{b_eq} using (4-4) for each harmonic order.

Chapter 5

Transient-based approach for harmonic impedance determination

With transient methods, harmonic impedance can be obtained over a wide range of frequencies. Steady-state methods are simple and also provide accurate information about harmonic impedances for long periods. By combining the advantages of each kind of method, an efficient composite technique can be developed with redundant information to provide reliable results. As was shown in the previous chapter, the steady-state program needs to know only where the disturbance occurs in order to select the pre- and post-disturbance cycles. For this approach, accurate detection of the transient is not required. On the other hand, for the transient method, a correct assessment of the transient is critical.

The chapter is organized as follows. In section 5-1, some theoretical background is provided regarding the characterization of transients due to capacitor switching. Section 5.2 presents a transient detection technique. Section 5.3 deals with sensitivity analyses regarding frequency resolution. Some sample results are provided in Section 5.4. Finally, the major findings are presented in Section 5.5.

5.1 Characterization of the capacitor switching transient

A transient is characterized by two parameters: magnitude and duration. In addition, this thesis presents a transient's characteristic harmonic content. A transient due to the switching of a capacitor has the following characteristics [39]:

- Magnitude: Up to 2 times the pre-existing voltage (assuming a discharged capacitor).
- Duration: From 0.3ms to 50ms (approx. 3 cycles).
- Main frequency component: 300Hz to 5 kHz.

The energization (isolated switching) of the capacitor bank used in this thesis typically generates a medium-frequency oscillatory voltage transient with a primary frequency between 300 and 900 Hz and magnitude of 1.3-1.5 pu, and not longer than two cycles.

5.2 Transient detection for harmonic impedance

Sophisticated methods are available to detect transients, such as modern artificial intelligence (AI) and wavelet transform [40]. Some other methods use criteria detection based on the absolute peak magnitude, the principal frequency and the event duration of less than 1 cycle [41]. This thesis presents a simple approach in the time domain that uses as criteria the sudden change (significant change between two consecutive points) in the capacitor current and the zero crossing of voltage to determine the amount of points per cycle.

Some other detection methods rely on the comparison of a 'normal-undisturbed' or predicted voltage waveform, with the actual one. If a waveform deviates from the predicted waveform by a value grater than a threshold, the transient is recorded [42].

Figure 5-1 shows how the module works for different thresholds, say 30%, 10%, and 5% respectively. This figure reveals that transient detection is very sensitive to the threshold chosen. Another disadvantage is that this module

calculates only the duration of the transient over the portion outside of the range predefined by the upper and the lower limits. Conversely, for the following proposed transient detection method, the definition of a threshold is not critical.

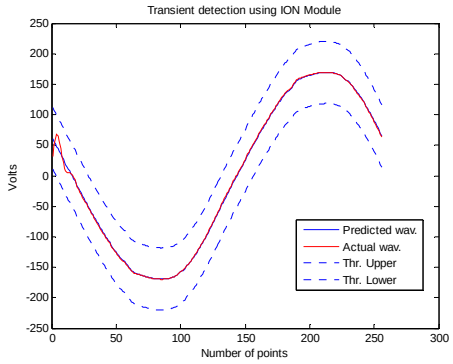

a. Threshold 30%.

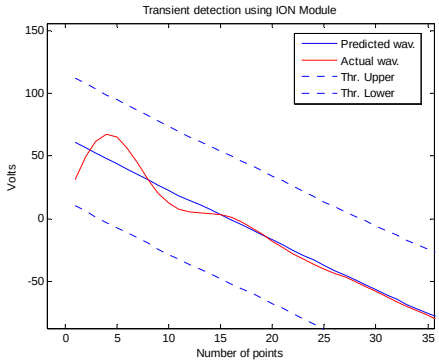

b. Zoom for Thr. 30%

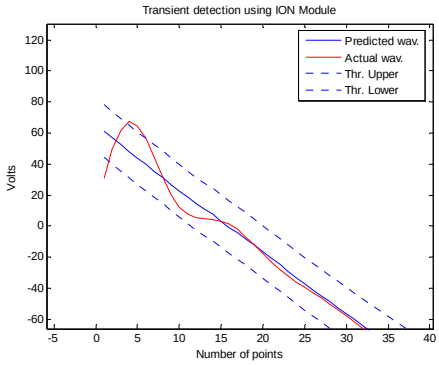

b. Zoom for Thr. 10%

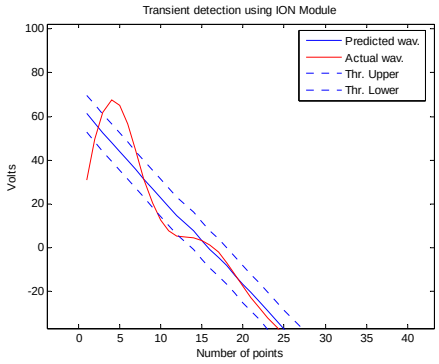

b. Zoom for Thr. 5%

Figure 5-1. Transient detection using different thresholds.

Figure 5-2 presents the subtracted waveform (derivative). This figure reveals the huge peak presented around the 1280th point (the sixth cycle). The advantage of taking the derivatives of the subtracted cycles is that a threshold to detect the beginning of the transient can be set up easily. For this case, the threshold was set up as three times the maximum value of the first two cycles.

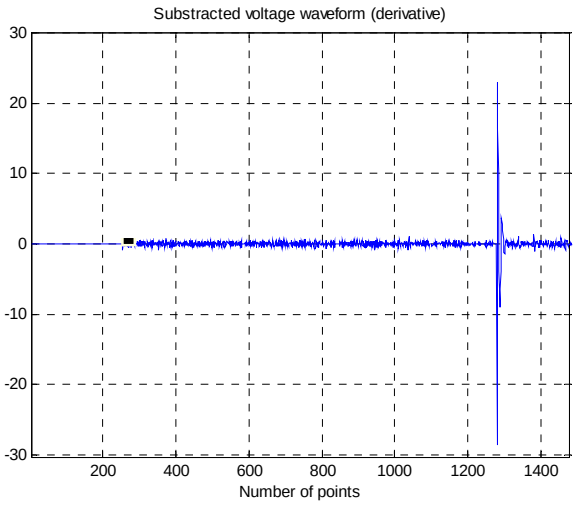

Figure 5-2 Derivative of the subtracted waveform (Voltage).

The idea behind this approach is that a transient due to, for instance, a capacitor switching generates a sudden change in the steady state conditions that can be numerically identified by using derivatives.

The transient signal is obtained by taking the moment the capacitor is switched on and subtracting a pre-disturbance cycle. Figure 5-3 presents the transient in the time domain.

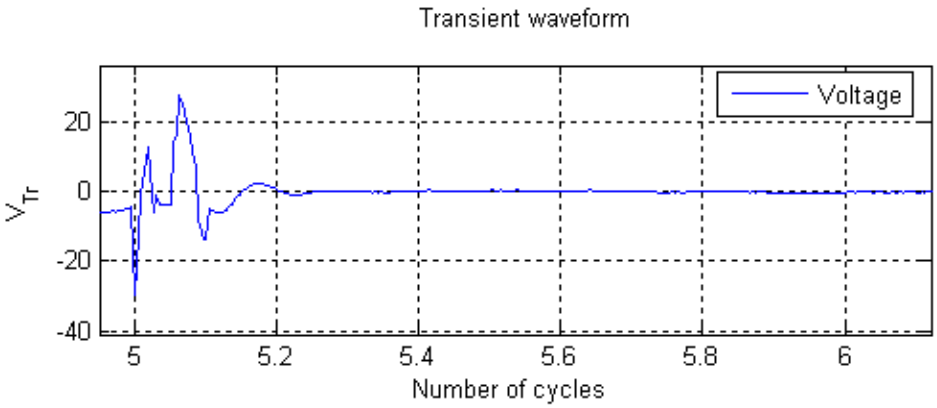

Figure 5-3 Extracted transient of the voltage signal.

As a consequence, the transient is calculated as

$$\begin{aligned} V_{tr} &= V_{Dist} - V_{\Pr e-dist} = \Delta V \\ I_{tr} &= I_{Dist} - I_{\Pr e-dist} = \Delta I \end{aligned} \quad . \tag{5-1}$$

Figure 5-4 presents the frequency content of a capacitor switching event. As expected, the higher frequency components (except the fundamental component) are around the 5th to 10th harmonic (300-600Hz).

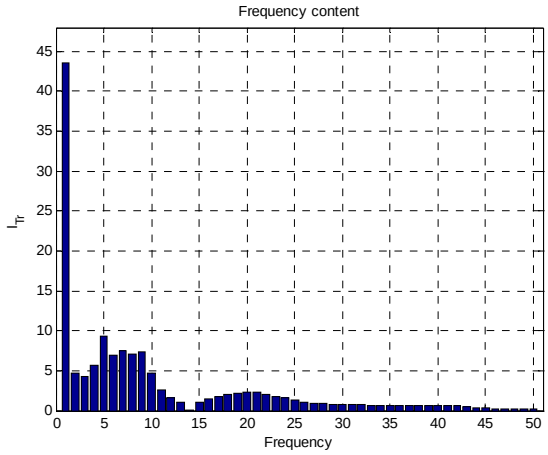

Figure 5-4 Frequency content of transient current

5.3 Windowing and frequency resolution

The data-window length has to be compromised between the frequency resolution and the proper window to entirely capture the transient event. The best choice of the data-window length is a length long enough to completely capture the transient and to provide sufficient frequency resolution [43].

Due to the characteristics of the acquired signals (15 cycles, 5 pre-disturbance), the higher frequency resolution is 15 Hz. The results using one cycle give a frequency resolution of 60Hz. Since we want to have a more refined

frequency resolution, one-cycle window results are not detailed here. Figures 5-5 and 5-6 show sample cases of measured transient voltage and transient current frequency spectra for the two- and three-cycle window length, respectively.

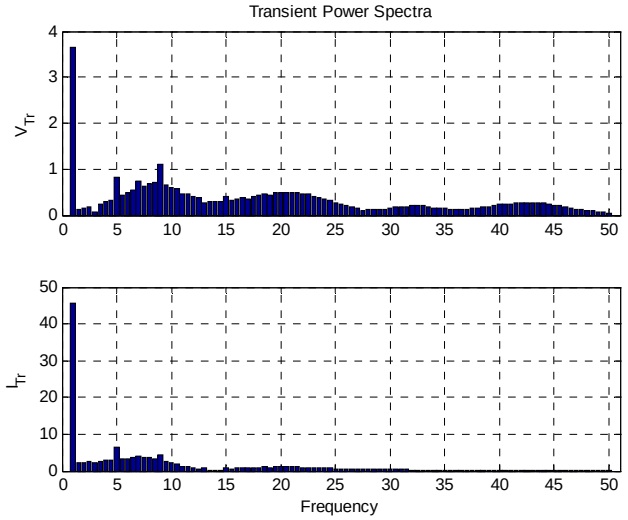

Figure 5-5 Two-cycle window length transient frequency spectra.

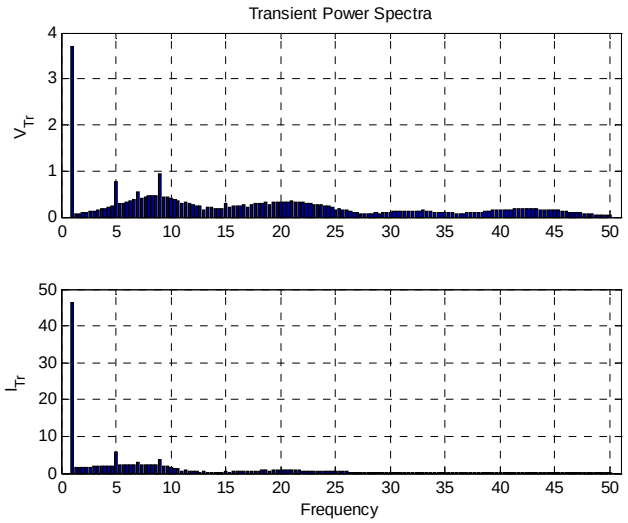

Figure 5-6 Three-cycle window length transient power spectra.

A proper data-window contains the entire transient event inside. After extensive field measurements, it was found that a two-cycle data window is long enough to capture the characteristics of the transient. For our application, if a longer data window had been used, no additional information would have been gained anyway. Figures 5-7 and 5-8 present the energy level for two- and three- cycle windows. For both cases, reliable results can be obtained within a range up to the 20^{th} harmonic (1200Hz). A longer data-window can yield fine frequency resolution, but also can reduce the power spectra density. The length of the data-window should be long enough to cover the entire transient without compromising the frequency resolution.

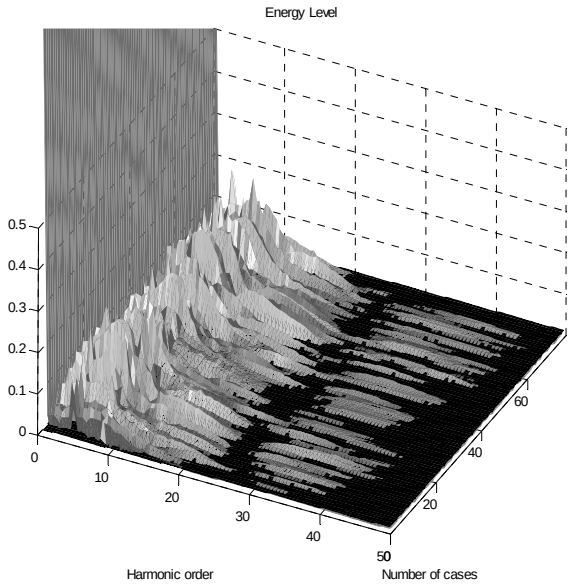

Figure 5-7 Energy level DI for two-cycle window length.

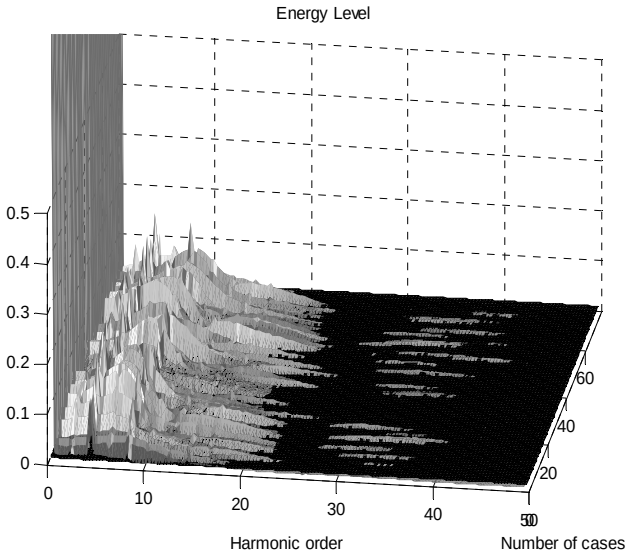

Figure 5-8 Energy level DI for three-cycle window length.

Figure 5-9 presents the comparative results for the harmonic impedances for different window lengths. The overall behavior of all cases is very similar (Figure 5-9a); however with a higher resolution, say 30 and 20 Hz, some slight differences occur (figure 5-9b). The results obtained with the two- and three- cycle windows are almost identical. These results validate that a window length of two cycles can be used for these harmonic calculations.

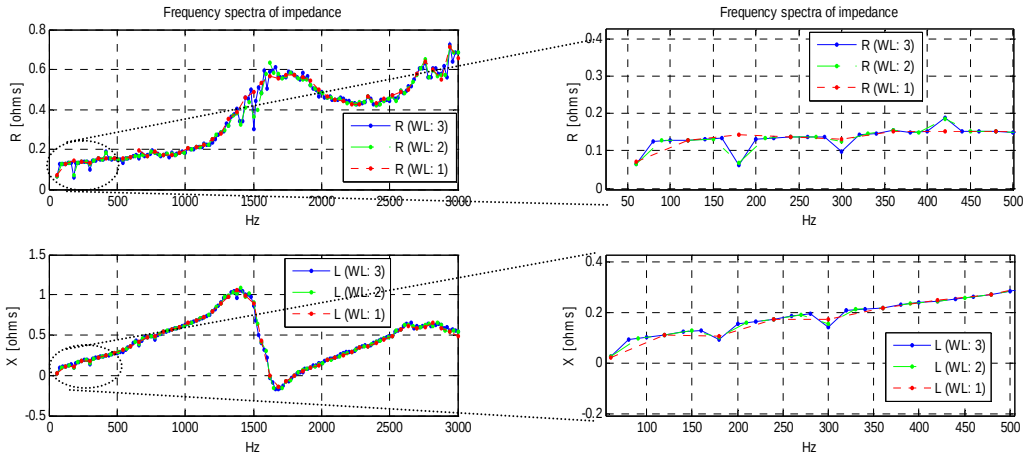

a. b.

Figure 5-9 Harmonic impedance with different window lengths: a. 60 – 3 kHz ; b. Zoom 60 – 500Hz.

5.4 Sample results and comparison with steady-state

As mentioned at the beginning of this chapter, with transient methods, harmonic impedance can be obtained over a wide range of frequencies. Steady-state methods are simple and also provide accurate information about harmonic impedances for long periods. By combining the advantages of each kind of method, an efficient composite technique can be developed with redundant information to provide reliable results.

From the all analyses describe above, Figures 5-10 to 5-12 present the impedance results obtained by using both methods. At the beginning of the frequency range, the values for both methods agree. The steady-state method provides good results depending on the system's harmonic background. These are discrete values and, in this case, are meaningless for frequencies above 600 Hz. The transient method provides information over a wider range of frequency. Close to 1000 Hz and above, the values become unreliable.

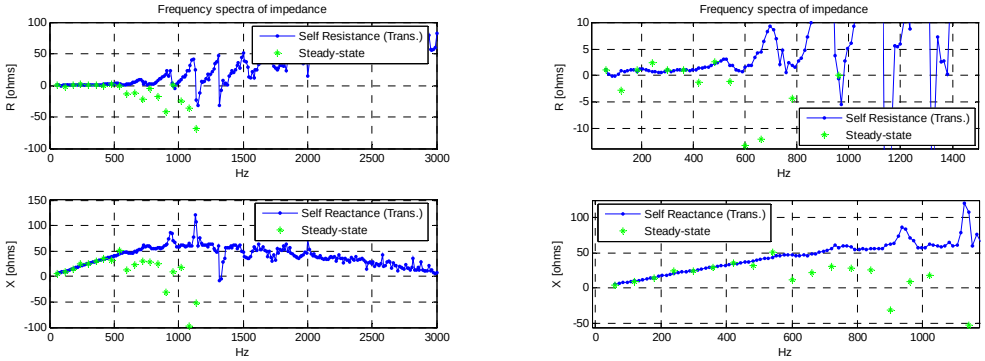

a. b.

Figure 5-10 Impedance results using Transient and Steady-state methods. a. The whole range of frequency, b. Zoom in up to 1kHz.

The steady-state approach provides values over only a short discretized frequency range depending on the system's harmonic background, as shown in Figure 5-11. When high energy levels are present (Figure 5-12), the harmonic impedance results agree with those obtained by using the transient method.

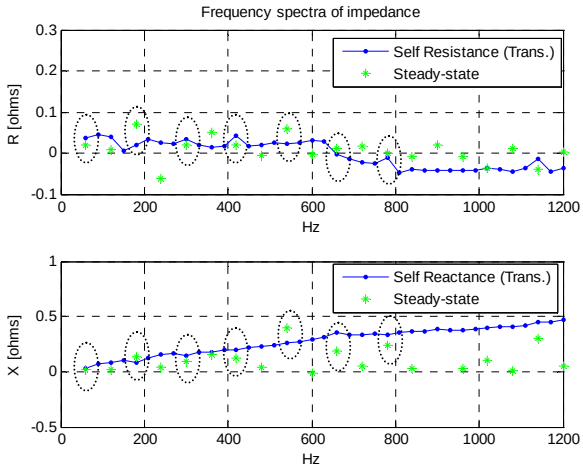

Figure 5-11. Impedance results for a sample case. Steady-state and transient method comparison.

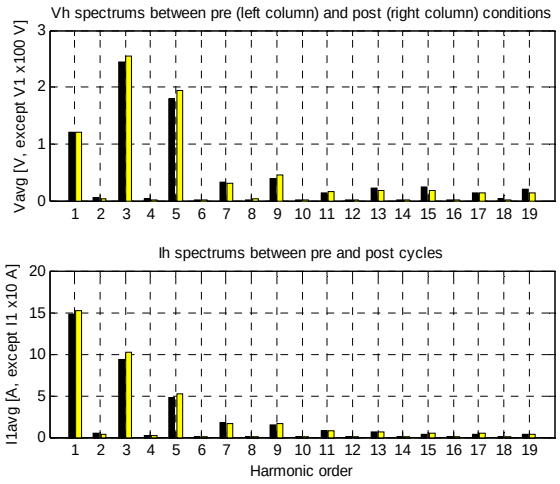

Figure 5-12. Frequency spectra for steady-state waveforms

5.5 Summary and major findings

This chapter presented a way to compute harmonic impedance by using transient-based methods. To use this approach, one must accurately acquire and detect the transient voltage and current. The proposed detection approach is effective and easy to implement, and the definition of a detection threshold is not as critical as it is for other methods.

By using two invasive methods - the steady-state and transient based methods- it was demonstrated to determine harmonic impedance can be determined consistently. Transient methods provide results over a wide range of frequencies, and steady-state methods provide good results depending on the system's harmonic background.

The process of developing the proposed algorithm can be summarized as

1. Input the phase voltage waveforms.
2. Subtract the first pre-disturbance cycle from the actual waveform.
3. Calculate the numerical derivative of the subtracted waveform.

4. Calculate the beginning of the transient by comparing the peak of the subtracted waveform with the maximum of pre-disturbance cycles. If a three-times change is found between two consecutive points, then the latter point of the transient is detected.
5. Extract the transients for both, voltage and current by using Equation 5-1.
6. Compute harmonic impedance $\left(-V_{tr}/I_{tr}\right)$.

Chapter 6

Case studies: Application of proposed technique over measured data

The previous chapters presented systematic techniques to estimate system-side and customer-side harmonic impedances and harmonic sources. This chapter presents the applicability of these proposed techniques to real measured data. Analyses over five residential single-phase supply cases are presented. The impedances and harmonic sources obtained from the mentioned sites have been examined. Section 6-1 presents the general characteristics of the measured sites. The utility and load side harmonic impedances are presented in Section 6-2 and Section 6-3, respectively. Section 6-4 presents harmonic distortion characteristics. Harmonic impedances will also be used for estimating the harmonic sources, which are presented in Section 6-5. Finally a summary of major findings is presented in section 6-6.

6.1 Characteristic of the measured sites

These measurements consist of several capacitor switching events. Each test site involves 20 to 60 capacitor switching events, called snapshots. Steady-state and transient data from each snapshot are used to calculate the harmonic impedances.

Table 6-1 summarizes the characteristics of the measured residential sites. Old and new houses with different sizes are included in this study.

Table 6-1 Characteristics of the measured houses.

House ID	Year Built	Square Footage [ft2]	No. of Inhabitants	THD Voltage [%]	THD Current [%]	Load [A] during test
1	1984	800	2	3.6	19.2	4.8
2	1976	1000	2	3.2	21.2	7.0
3	1997	2000	4	1.6	27.4	6.1
4	2003	1800	2	3.4	29.2	8.9
5	1985	1200	4	2.7	19.6	10.8

6.2 Characteristics of Utility-system Harmonic Impedances

From the sample cases presented in the chapter 3, particularly in figure 3-12, it was found that impedances for the utility-side consistently exhibit linear increasing characteristics with respect to the harmonic frequency. As a result, it is reasonable to assume that impedances follow the following linear equation:

$$\begin{aligned} R(h) &= a_R h + b_R \\ X(h) &= a_X h + b_X \approx a_X h \end{aligned} \tag{6-1}$$

where h is the harmonic number. According to the circuit theory, the reactance should be zero when h=0. So bx is set to zero. Parameters a_R, b_R and a_X are determined using the least square fitting method by minimizing the following functions:

$$\begin{aligned} \varepsilon_R &= \sum w_R(h)\left[R_h - R(h)\right]^2 = \sum w_R(h)\left[R_h - (a_R h + b_R)\right]^2 \\ \varepsilon_X &= \sum w_X(h)\left[X_h - X(h)\right]^2 = \sum w_X(h)\left[X_h - (a_X h)\right]^2 \end{aligned} \tag{6-2}$$

where R_h and X_h are the mean values, w_R and w_X are the weighting factors for R and X respectively. The weighting factors are the confidence levels of the data. The confidence level shows the percentage of snapshots that are within an acceptable error. In our study, the maximum acceptable error is limited to ten percent. Results obtained for one of the measured sites is shown in Figure 6-1. This figure shows the

mean value for *R* and *X*, and the associated confidence levels. The circle-dotted points represent the results whose confidence levels are higher than 25%.

Using this process, the harmonic impedances of each site can now be characterized in a compact form using just three parameters: a_R, b_R and a_X.

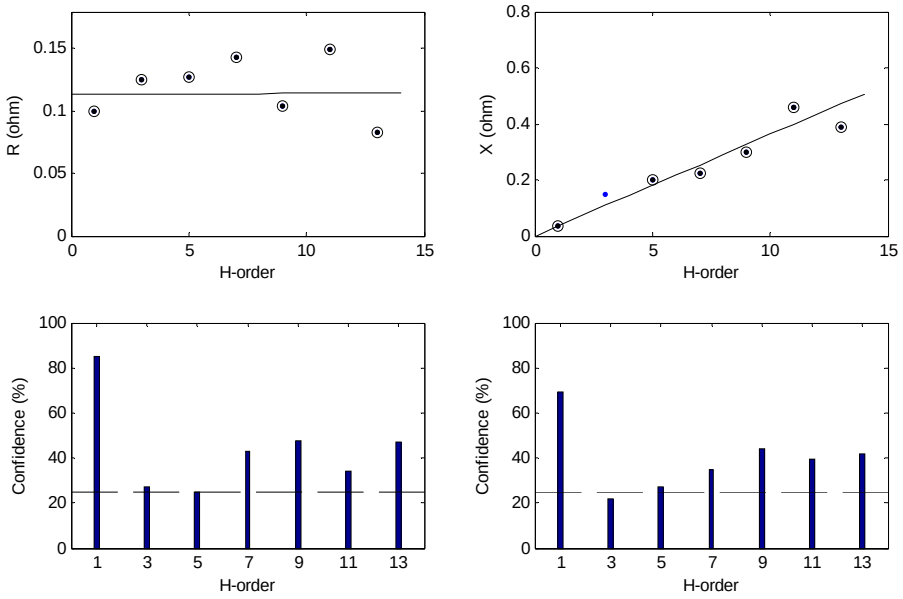

Figure 6-1 Representative values for harmonic impedances.

In order to compare the harmonic impedances among the measured sites to determine the general impedance characteristics for all sites, the harmonic impedance of each site was normalized based on the fundamental frequency components of *R* and *X* as follows:

$$R_{ratio}(h) = \frac{R(h)}{R_1} = \frac{a_R h + b_R}{R_1} = a'_R h + b'_R$$
$$X_{ratio}(h) = \frac{X(h)}{hX_1} = \frac{a_X h}{hX_1} = a'_X \qquad (6\text{-}3)$$

The above normalization is equivalent to performing per-unit conversion on the data. If the impedance follows the form of $Z(h)=R+jhX$, the normalized impedance will be $Z(h)'=1+j1$. As a result, this conversion brings two advantages: 1) we can compare the normalized impedances for different sites and 2) the ideal values (or expected values) of the normalized impedances are known, which are $a'_R=0$, $b'_R=1$ *and* $a'_X=1$. As a result, the supply system harmonic impedance seen at the custom revenue meter point follows a linear relationship based its 60Hz impedance, i.e.

$$Z(h)=R_{60Hz}+jhX_{60Hz} \tag{6-4}$$

Table 6-2 presents the results obtained for the measured sites. Parameters a_R, b_R and a_X are close to their expected values which validates the assumption of linear harmonic impedances. The least two columns show the least-square fit errors.

Table 6-2 Normalized harmonic impedance parameters for measured houses.

Site	$R_1[\Omega]$	$X_1[\Omega]$	a'_R	b'_R	a'_X	εR (%)	εX (%)
1	0.0997	0.0357	0.0005	0.9995	1.0167	7.45	5.64
2	0.0497	0.0161	0.0253	0.9747	0.9589	3.28	3.11
3	0.1082	0.0499	0.0053	0.9947	0.9719	5.69	1.43
4	0.0535	0.0163	0.0439	0.9561	1.2359	5.15	6.54
5	0.1661	0.0412	0.0153	0.9847	1.0322	3.99	1.63

6.3 Characteristics of Load-side Harmonic Impedances

Figure 6-2 shows the average resistance and (absolute) reactance values as a function of harmonic frequency. This figure reveals that the resistive component dominates the load-side impedance. Both R and $|X|$ increase slightly with the frequency. At the fundamental frequency, the load impedances are much higher and, so one cannot use the fundamental frequency impedance to predict the

harmonic impedance of the loads. In Figure 6-2 the load impedances are also compared with the average system impedance. The results show that the load impedances are higher than the system impedances, at least to the 13th harmonic.

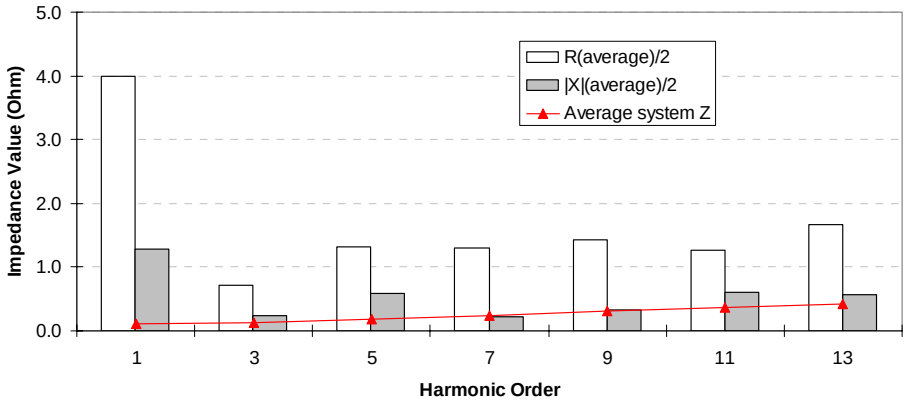

Figure 6-2 General frequency-dependent response of load side impedances.

From among all measured sites, some specific cases related to residential customers were chosen for presentation in this section. Figure 6-3 presents the impedance results (*R* and *X*) for a sample house for each branch. The resistance component shows a fairly constant trend for the harmonic orders. On the other hand, the reactance increases with the frequency. The results obtained by using steady-state and transient data are also consistent.

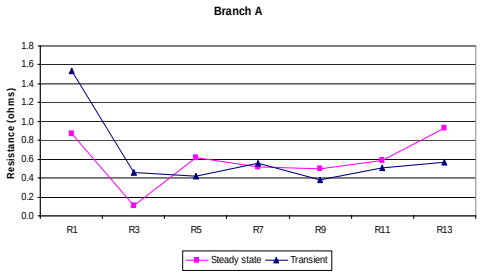

a.

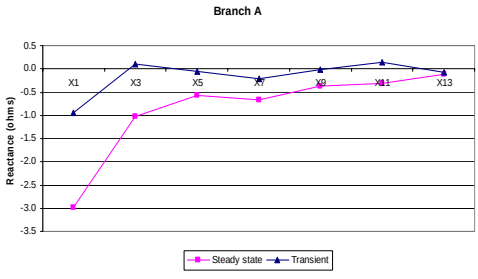

b.

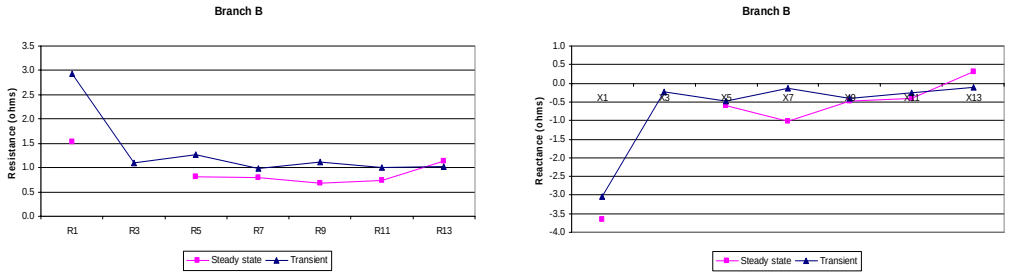

c. d.

Figure 6-3 Sample load impedance results: a. and b. R and X for branch A; c. and d. R and X for branch B.

Figures 6-4 to 6-8 present the impedance results for four different houses. In most of the cases, the impedances present a capacitive characteristic. This result is not surprising since the capacitors in the power electronic-based loads have been previously found to create such a characteristic [44].

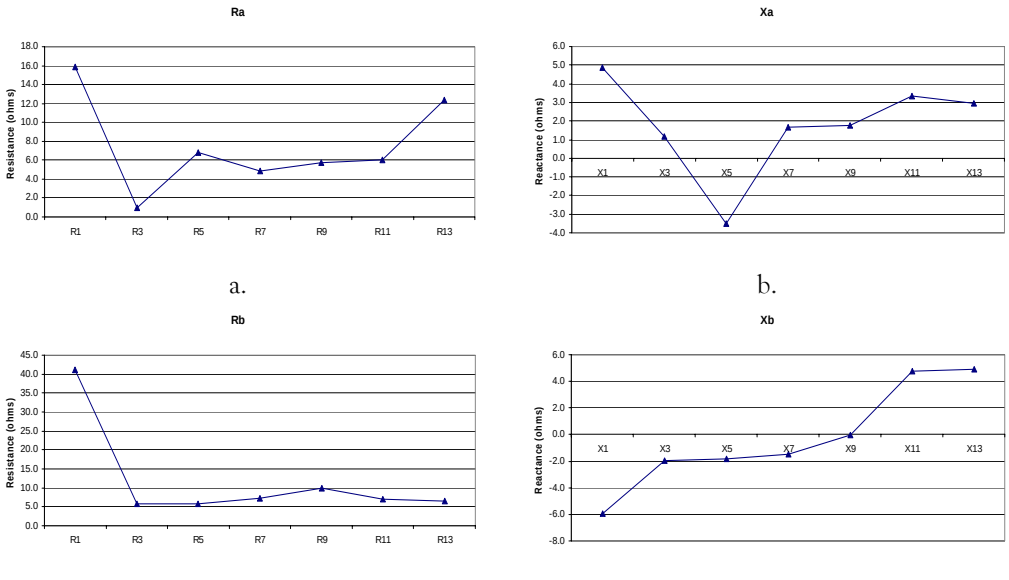

a. b.

c. d.

Figure 6-4 Load impedance results for house # 1.

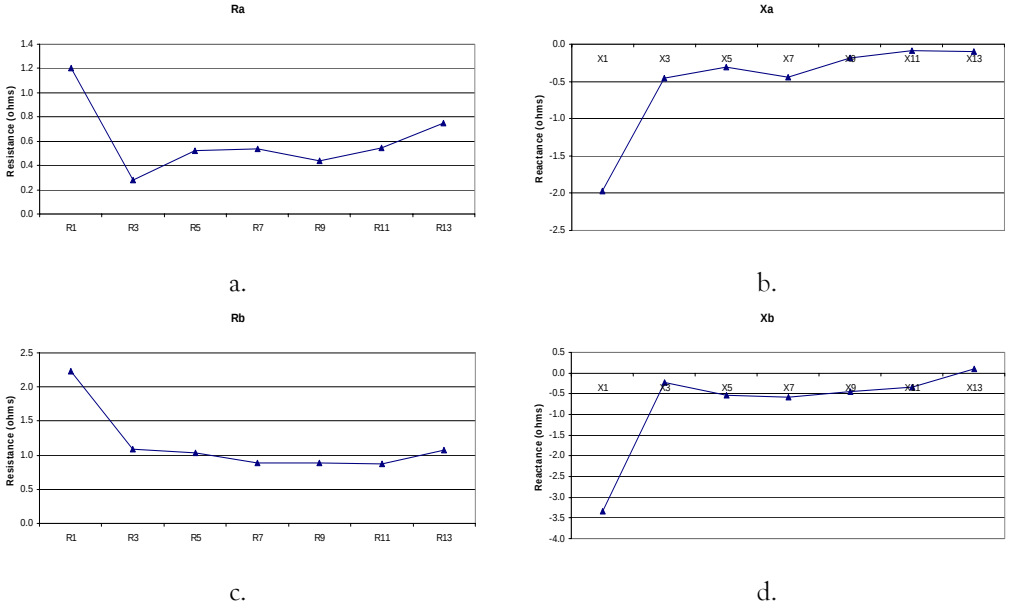

a. b.

c. d.

Figure 6-5 Load impedance results for house # 2.

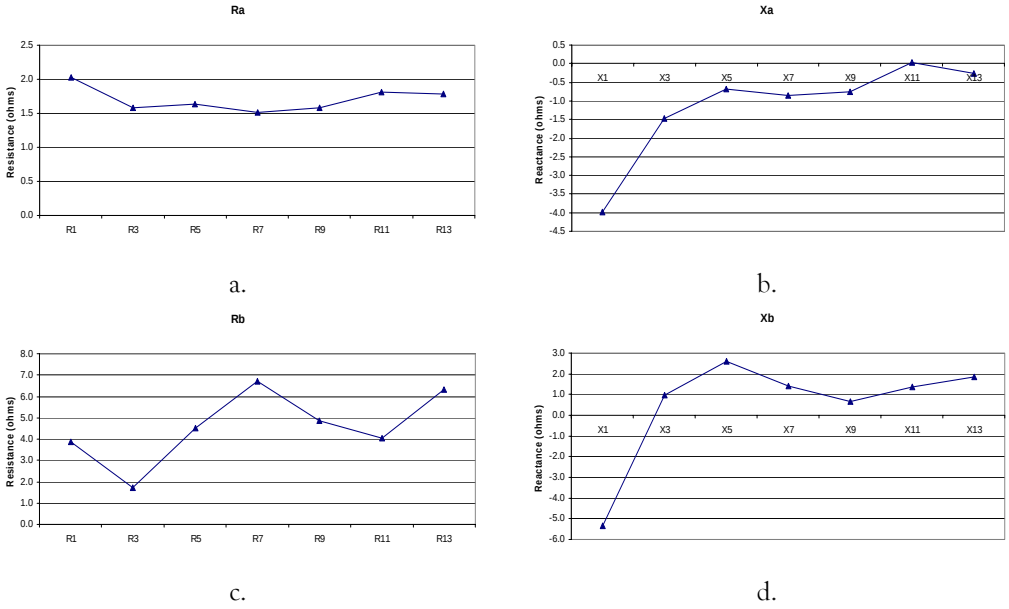

a. b.

c. d.

Figure 6-6 Load impedance results for house # 3.

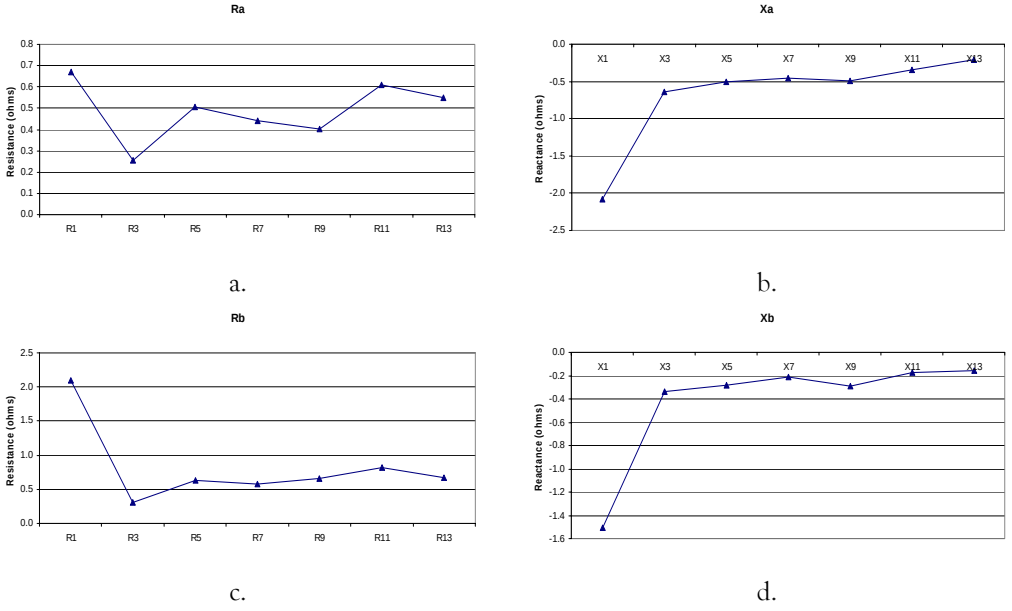

a. b.

c. d.

Figure 6-7 Load impedance results for house # 4.

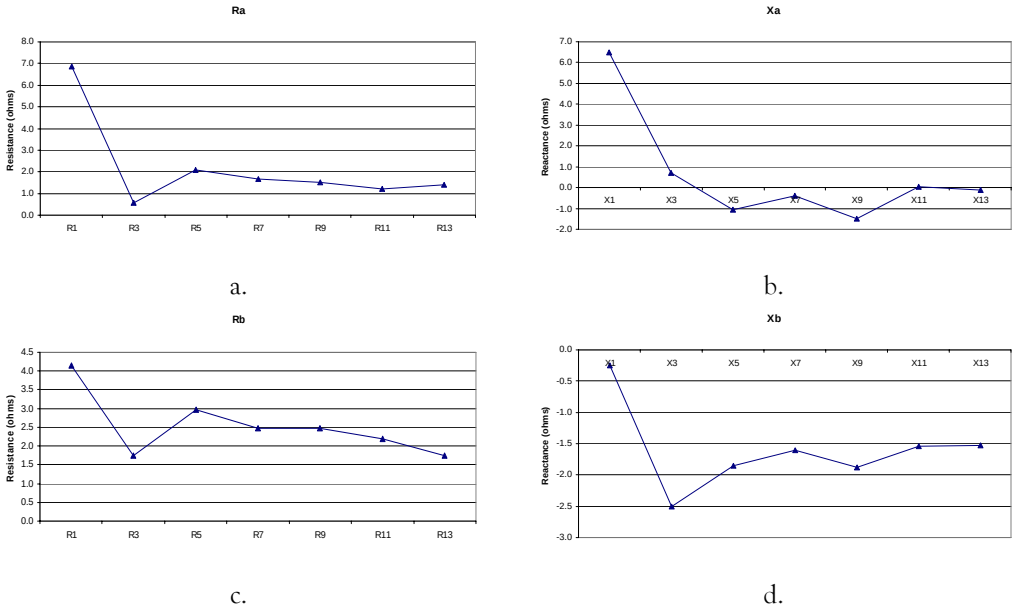

a. b.

c. d.

Figure 6-8 Load impedance results for house #5.

In general and as stated at the beginning of this section, for all sites, *R* is bigger than X. However, the results did not yield consistent conclusions. So it is not clear what affects the frequency response characteristics of the loads.

6.4 Harmonic Distortion Characteristics

Harmonic distortions characteristics of the measured sites will help to understand the characteristics of the parameters obtained. At each site, currents and voltages of all phases are processed. Table 6-3 summarizes the key indices for all sites. The average voltage distortion of the test sites is about 2.91% and THD as high as 3.6% have been recorded. The voltage distortions are mainly caused by the 3rd and 5th harmonics.

Table 6-3 PCC indices for measured sites.

Indices	Site 1	Site 2	Site 3	Site 4	Site 5
Power consumption [W]	535.55	813.86	704.91	1027.48	1235.62
Fundamental power factor	0.9561	0.9766	0.9843	0.9886	0.9671
Current [A]	4.7888	7.0179	6.1150	8.8991	10.8346
Voltage THD [%]	3.60	3.20	1.62	3.40	2.71
3rd Harmonic Voltage [%]	2.86	1.96	0.97	2.25	1.47
5th Harmonic Voltage [%]	1.82	2.21	1.04	2.32	2.07
7th Harmonic Voltage [%]	0.76	0.96	0.46	0.66	0.32
9th Harmonic Voltage [%]	0.76	0.67	0.42	0.72	0.81
11th Harmonic Voltage [%]	0.39	0.25	0.45	0.22	0.24
13th Harmonic Voltage [%]	0.40	0.25	0.15	0.33	0.28
Voltage Crest Factor	1.37	1.37	1.39	1.37	1.39
Current THD [%]	19.21	21.18	27.36	29.25	19.61
Current TDD* [%]	0.90	1.46	1.61	2.50	2.08
3rd Harmonic Current* [%]	0.69	1.12	1.20	2.01	1.70
5th Harmonic Current* [%]	0.46	0.80	0.81	1.33	1.12
7th Harmonic Current* [%]	0.25	0.39	0.53	0.57	0.42
9th Harmonic Current* [%]	0.19	0.14	0.40	0.05	0.03
11th Harmonic Current* [%]	0.12	0.12	0.24	0.19	0.17
13th Harmonic Current* [%]	0.11	0.18	0.09	0.24	0.10
Current Crest Factor	1.78	1.78	2.03	1.96	1.76

* The TDD and harmonic current [%] is based on a rated current of 100A.

Figures 6-9 and 6-10 show the harmonic voltage and current spectrum of one of the sites, respectively. Figure 6-11 shows the current THD and Figure 6-12

shows the Crest Factors of the sites (Crest Factor of 1.414 represents a perfect sinusoid). The average current distortions are 23.32% THD. Note that this number is affected by the denominator used for the calculations. The index is therefore not as meaningful as the voltage THD. The IDD index reveals that the 3rd harmonic is the main component of the current harmonics, which is then followed by the 5th and 7th harmonic.

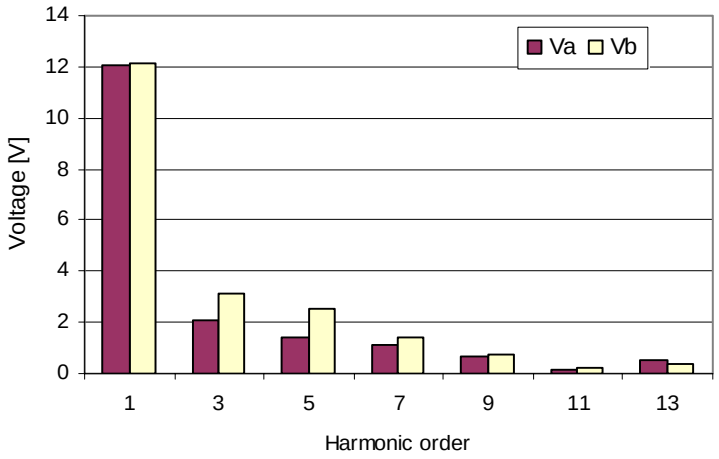

Figure 6-9 Harmonic spectrum of voltages at the PCC (V_1 is divided by 10).

Figure 6-10 Harmonic spectrum of currents measured at the PCC (I_1 divided by 10).

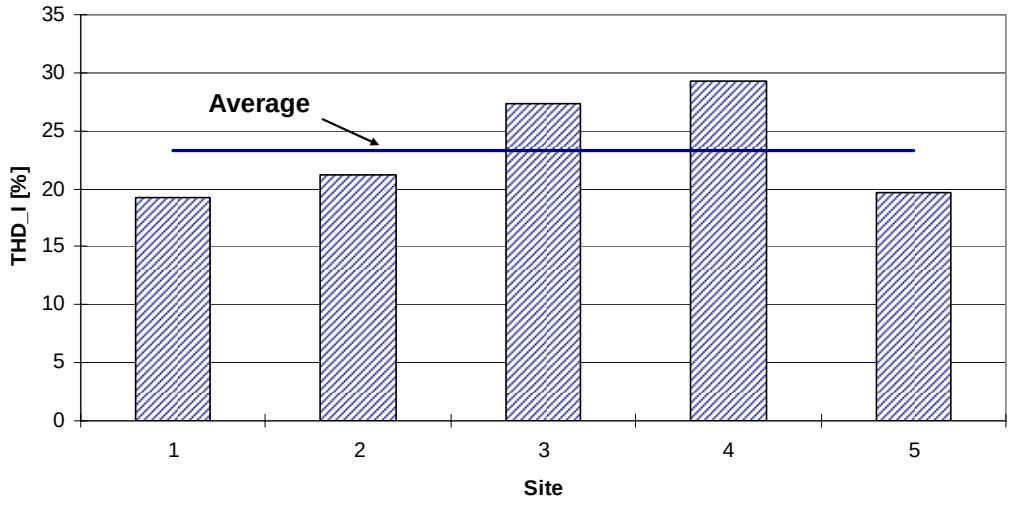

Figure 6-11 Current THD (%) at the PCC.

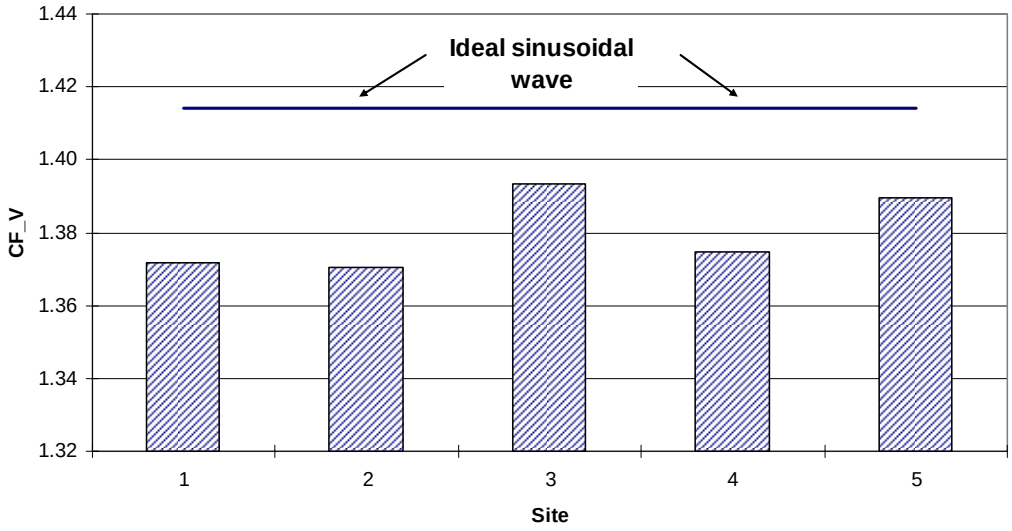

Figure 6-12 Voltage crest factors of measured sites.

Based on the TDD results, it was found that the loads measured by this project inject an average of 1.55 amperes of 3rd and 1.04 amperes of 5th harmonic currents into the system.

The Crest factor results reveal that the majority of sites have current waveforms that are spike shaped as most of the sites have a CF greater than 1.414. On the other hand, most voltage waveforms are flat-topped (CF<1.414).

Figures 6-13 and 6-14 compare the harmonic distortion levels for the measured sites. It was found that the voltage THDs and current TDDs are generally comparable.

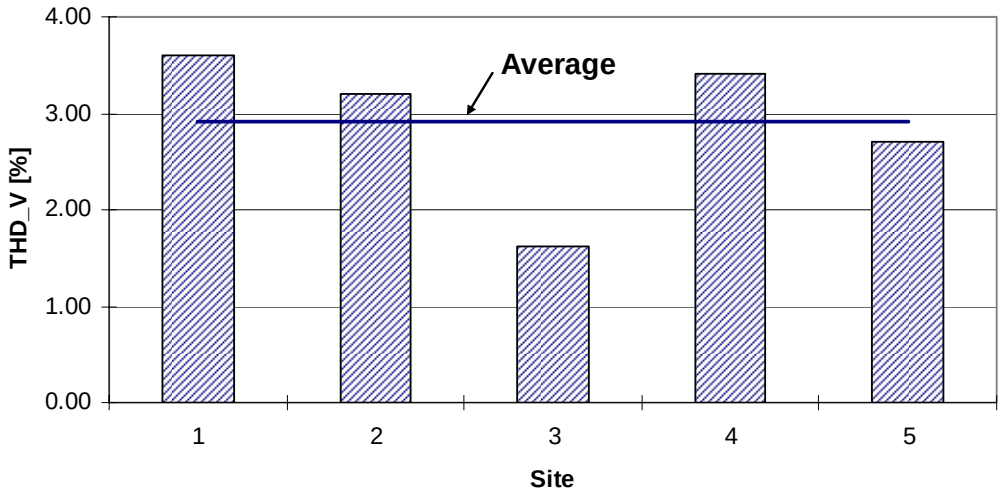

Figure 6-13 Impact of Voltage THD.

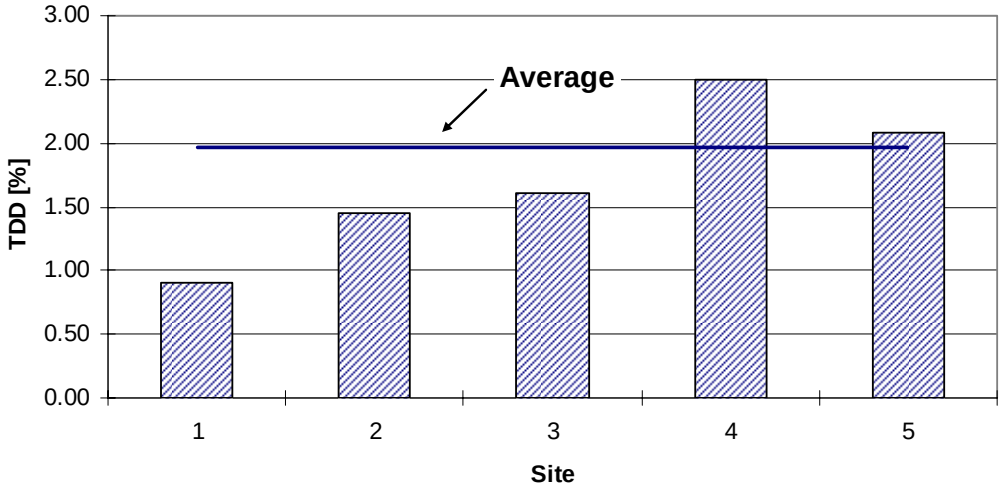

Figure 6-14 Impact of Current TDD.

To understand this observation in more detail, the distribution of the 3rd, 5th, 7th and 9th harmonic currents are shown in Figure 6-15. The charts reveal that the excessive harmonic current injection is mainly caused by the 3rd and to some extent by the 5th harmonics.

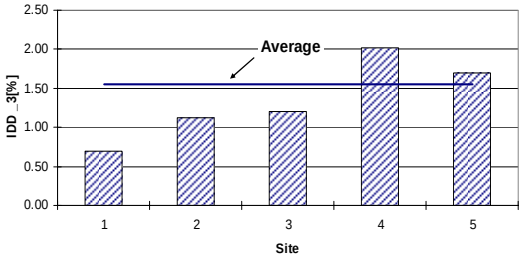

a. 3rd harmonic current IDD

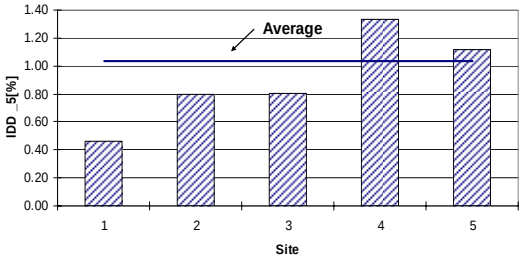

b. 5th harmonic current IDD

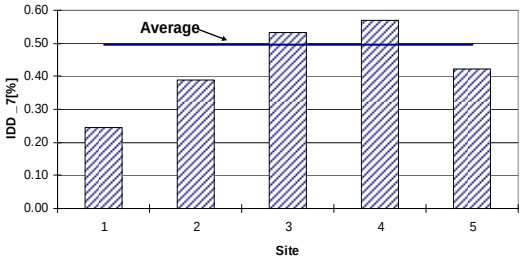

c. 7th harmonic current IDD

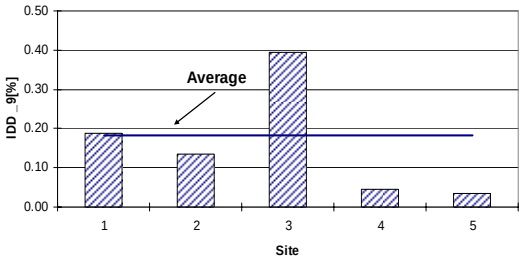

d. 9th harmonic current IDD

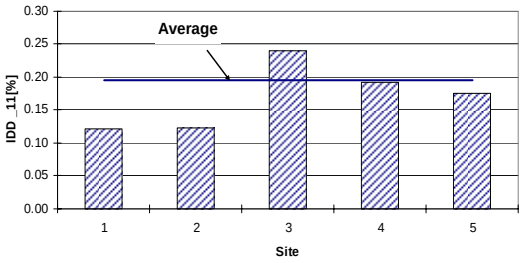

e. 11th harmonic current IDD

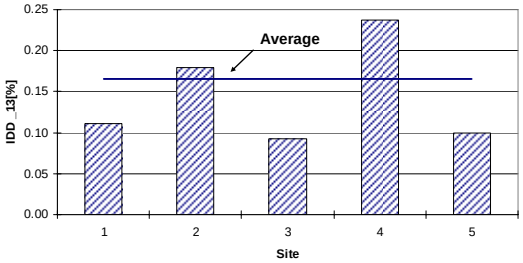

f. 13th harmonic current IDD

Figure 6-15 Impact of IDD for harmonic orders.

6.5 Characteristics of the harmonics sources

Based on the impedances of the system and load sites, we can estimate the harmonic sources inside the system and the load. The results will help to identify the causes of harmonic distortions, voltage and current, at the system-load interface points. System and customer side harmonic sources are determined for measurement sites from available impedance information. The characteristics of the sources are analyzed.

6.5.1 Characteristics of Utility Side Sources

This section investigates the characteristics of utility side harmonic source *Eu* and correlates the findings with the PCC voltages. Table 6-4 summarizes the overall characteristics of *Eu*.

Table 6-4 Utility side source characteristics.

Indices	Site 1	Site 2	Site 3	Site 4	Site 5
Voltage [V]	120.05	121.90	123.06	121.71	121.36
Voltage THD [%]	3.52	3.18	3.33	1.60	2.58
3rd Harmonic Voltage [%]	2.81	1.95	2.21	0.95	1.39
5th Harmonic Voltage [%]	1.75	2.20	2.27	1.02	1.96
7th Harmonic Voltage [%]	0.76	0.95	0.63	0.45	0.26
9th Harmonic Voltage [%]	0.75	0.67	0.71	0.41	0.80
11th Harmonic Voltage [%]	0.36	0.25	0.21	0.44	0.27
13th Harmonic Voltage [%]	0.39	0.25	0.32	0.15	0.27

The characteristic analysis conducted for *Vpcc* has been done for *Eu*. Figure 6-16 compares the harmonic spectra of V_{pcc} and E_u for average values obtained from all sites. The charts show that the patterns of E_u and V_{pcc} spectra are similar, further confirming that E_u has a major influence on V_{pcc}. This is, the PCC voltage distortion is caused by the harmonic voltage sources inside the system.

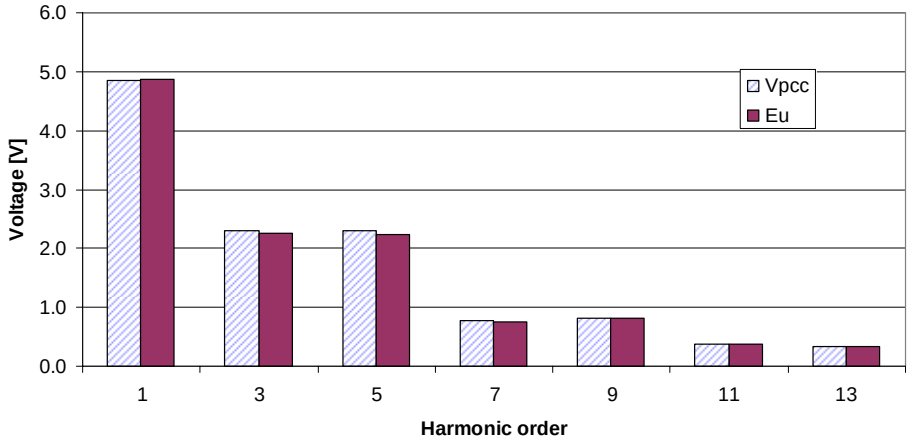

Figure 6-16 Comparison of harmonic spectra of E_u and V_{pcc} (V_1 divided by 25).

6.5.2 Characteristics of Customer Side Sources

The customer side sources are represented as current sources I_c. Table 6-5 summarizes the overall characteristics of I_c. Again the similarities between I_{pcc} and I_c are noticed. In order to investigate these similarities further, the harmonic spectral of I_{pcc} and I_c are compared in Figure 6-17.

The spectral results reveal that the patterns of I_c and I_{pcc} are similar. However, this similarity cannot confirm that I_{pcc} is mainly affected by I_c since they represent the most common spectra patterns seen in a power distribution system; however, the harmonic currents recorded at the revenue meter point are not entirely caused by the nonlinear loads inside the customer's facility. How to determine to what extent the system affects the PCC current is out of the scope of this work.

Table 6-5 Characteristics of harmonic current sources I_c.

Indices	Site 1	Site 2	Site 3	Site 4	Site 5
Current rms [A]	6.8445	94.0731	43.4307	97.6511	28.1720
Current TDD* [%]	2.17	12.17	4.79	2.64	3.75
3rd Harmonic Current* [%]	1.83	8.06	3.44	1.92	3.22
5th Harmonic Current* [%]	1.02	7.70	3.01	1.41	1.60
7th Harmonic Current* [%]	0.42	4.01	1.11	0.88	0.63
9th Harmonic Current* [%]	0.30	2.45	0.65	0.50	0.77
11th Harmonic Current* [%]	0.21	0.89	0.39	0.32	0.24
13th Harmonic Current* [%]	0.16	1.07	0.47	0.41	0.26

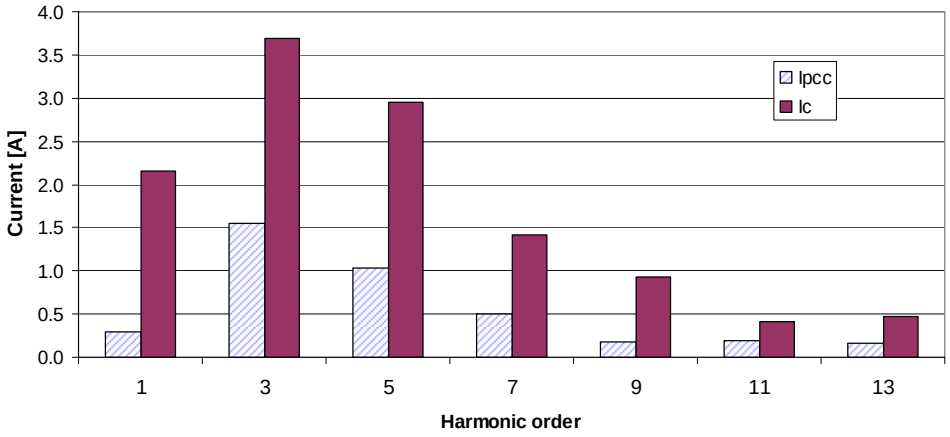

Figure 6-17 Comparison of harmonic spectra of I_c and I_{pcc} (I_1 divided by 25).

6.6 Summary of major findings

This chapter has shown the utility and load side impedance estimates and the results have revealed some interesting characteristics of the loads from information that is relatively easy to obtain (usage of same set of data harmonic impedance estimation at both sides of the interface point).

In addition, it has proven the validity of the linear impedance assumption through measured field data. Utility-side impedance can be represented by a linear model. On the other hand, load impedances had no general frequency response characteristics. It was found, however, that some loads exhibited capacitive impedance at certain frequencies, likely because of the capacitors inside the power-electronic based appliances. Also, the fundamental component impedances were higher than those of the harmonic components.

It is possible to see from the characteristics of harmonic distortions at the utility-customer interface point that the 3rd harmonic currents are becoming significant harmonic component in residential systems. The majority of the sites measured have the 3rd harmonic current as the dominant harmonic current

component. The voltage distortion is still dominated by the 5th harmonic but this may change if more and more 3rd harmonic current producing loads are installed in the system.

Intuitively, the voltage distortions are produced by the collective impact of various loads. On the other hand, the current harmonics are affected by the load characteristics, which suggests that a large portion of the harmonic currents observed at the PCC are due to the loads connected to the PCC.

The crest factor results reveal that the majority of sites have current waveforms with a spike shape. On the other hand, the major part of voltage waveforms are flat-topped. This has been observed in other measurement sites, seems to be very general and can be applied to all distribution systems.

Regarding the characteristics of harmonic sources inside the utility and customer systems, the results show that the harmonic voltages at the PCC are mainly determined by the utility side harmonic sources. These sources are the collective result of the multiple harmonic producing loads distributed across a distribution system. If a customer harmonic current has any direct impact on its PCC voltage, it likely to be more noticeable at the 3rd harmonic. On the other hand, results show that the PCC currents are affected by both the utility side and customer side harmonic sources. More studies are needed to quantify the relative impact of each source.

In summary, the characteristics of *Eu* are similar to those of *Vpcc*. These similarities seem to reinforce the belief that the utility side harmonic sources have significant effect on the PCC voltage distortion.

Chapter 7

Contributions and Conclusions

7.1 Harmonic impedance

This thesis presented a practical and systematic technique to determine one of the key harmonic parameters in power systems, *harmonic impedance*. The estimation was performed in the frequency domain for low-voltage customers, who usually are supplied through single-phase transformers. The thesis' main objective was to expand and complete the harmonic impedance and harmonic source measurement methodology under energized conditions.

The utility- and load-side impedance results were estimated from the same set of data at both sides of the interface point. The proposed methodology uses a simple portable capacitor bank to create waveform changes for impedance determination. The results show that a capacitor-sized round 1mF is sufficient for measuring most residential customers.

By using two invasive methods, the steady-state and transient based methods, it was demonstrated that harmonic impedance can be determined consistently. Transient methods provide results over a wide range of frequencies, and steady-state methods provide good results depending on the system's harmonic background.

The energies of the disturbance available to determine the load site impedances were much smaller than those for system-side impedance determination. Therefore, the load impedance results were much more scattered

among the various snapshots and therefore less accurate that the results obtained for the system-side impedance. This result occurred because most of the capacitor-switching transients travel to the system side (the smaller impedance) instead of the load side.

Finally, the utility-side impedance characteristic represented by a linear model was proven through measured field data. This linear relationship is based on the fundamental power frequency, i.e., $Z(h)=R_{60Hz}+jhX_{60Hz}$. Conversely, load impedances had no general frequency response characteristics, but some loads presented capacitive impedance at certain frequencies due to the capacitors inside the power-electronic based appliances.

Customer loads can be represented by Norton equivalent circuits at different harmonic frequencies. The equivalent impedances showed that the resistive component dominated the load impedance. The impedance values were higher than those of the supply systems at low-order harmonics.

7.2 Harmonic distortion characteristics and harmonic sources

In addition to and based on the harmonic impedances results, harmonic distortion analyses, and the equivalent harmonic sources of the supply system and the customer loads were also determined. The third harmonic currents are becoming a significant harmonic component in residential systems at the PCC. Most of the measured sites show the 3rd harmonic current as the dominant harmonic current component. For the voltage distortion, the 5th harmonic is the dominant, but this situation may change if more and more 3rd harmonic current-producing loads are installed in the system.

Regarding the characteristics of the harmonic sources inside the utility and customer systems, the results showed that the harmonic voltages at the PCC were determined mainly by the utility side harmonic sources. These sources are the collective result of the multiple harmonic-producing loads distributed across a distribution system. If a customer's harmonic current has any direct impact on its PCC voltage, it is likely to be more noticeable at the 3rd harmonic. Additionally, it was also found that the PCC currents were affected by both the utility-side and customer-side harmonic sources.

The harmonic current caused by the loads has no control over the voltage distortion. The same load located in two different points in the power system may result in two different voltage distortion profiles.

7.3 Recommendations and future research

Working with real measurements significantly increases the difficulty level of power system parameter estimation. Implementation issues such as the energy of the disturbance, phase shift, channel synchronization and load variation have an important influence on the reliability of the results.

The accurate estimation of harmonic impedance is fundamental in characterizing frequency responses and harmonic propagations, and assessing harmonic limits. Furthermore, harmonic impedance studies are important stepping stone for developing potential applications such as harmonic sources determination, which has been explored in this work.

The other potential application is the determination of harmonic contributions. The results presented here show that the PCC currents are affected by both the utility-side and customer-side harmonic sources. Future research could

focus on quantifying the relative impact of each source. After the harmonic sources contained in both the customer and utility systems have been determined, the harmonic contributions due to a customer and its supply system would be the next step in the harmonic analysis.

Although the harmonic currents produced by individual appliances are small, the cumulative effect produced by a large number of small harmonic sources can be substantial. Harmonic contributions based on field measurement will reveal how the amount of a customer's actual harmonic impact will be and the background harmonics' impact in the utility supply system.

References

[1] John D. Kueck and Brendan J. Kirby, *Measurement Practices for Reliability and Power Quality*. Oak Ridge National Laboratory, June 2004.

[2] Frank Jay, *The IEEE Standard Dictionary of Electrical and Electronics Terms*, Institute of Electrical and Electronics Engineers, New York, 1988.

[3] Roger C. Dugan, Mark F. McGranaghan, Surya Santoso and H. Wayne Beaty, *Electrical Power Systems Quality*. MC Graw-Hill, New York, 1996.

[4] C. Sankaran, *Power Quality*. CRC Press LLC, Florida 2002.

[5] Heydt G. T., *Contemporary Topics in Electric Power Quality - Tutorial on Harmonics*. Arizona State University, 2000.

[6] G. W. Chang., Chapter 2: Harmonics Theory, Tutorial on Harmonics Modeling and Simulation, IEEE Power Engineering Society, 1998.

[7] F. C. De La Rosa, Harmonics and Power Systems, Taylor & Francis Group, CRC Press, NW, 2006.

[8] "Modeling and simulation of the propagation of harmonics in electric power networks. Part I: Concepts, models, and simulation techniques", Task Force on Harmonics Modeling and Simulation, IEEE Transactions on Power Delivery, Vol. 11, No. 1, pp.452- 465, January 1996.

[9] "Modeling and simulation of the propagation of harmonics in electric power networks. Part II: Sample systems and examples", Task Force on Harmonics Modeling and Simulation, IEEE Transactions on Power Delivery, Vol. 11, No. 1, pp.466- 474, January 1996.

[10] IEEE Std. 519-1992: IEEE recommended practices and requirements for harmonic control in electrical power systems, 1992.

[11] IEC 61000-3-6: Electromagnetic compatibility (EMC), (1996-10).

[12] Greenwood A., *Electrical transients in power systems*, 2nd Edition, 1991, John Wiley & Sons.

[13] A. Robert and T. Deflandre, "Guide for assessing the network harmonic impedances," Joint CIGRE/CIRED 97,2-5 June 1997, Conference Publication No. 438, IEE, 1997.

[14] B. Palethorpe M. Sumner D. W. P. Thomas, "Power System Impedance Measurement using a Power Electronic Converter" Harmonics and Quality of Power, 2000. Proceedings. Ninth International Conference. Vol. 1, Oct. 2000, pp.208 – 213.

[15] Harris, M.B., Kelley A.W., Rhode J.P. and Baran, M.E.; "Instrumentation for measurement of line impedance" Applied Power Electronics Conference and Exposition, 1994. APEC '94. Conference Proceedings 1994, Ninth Annual, vol.2, Feb. 1994, pp.:887 – 893.

[16] Morched, A.S. and Kundur, P., "Identification and Modeling of Load Characteristics at High Frequencies", IEEE Transactions on Power Systems, Vol. PWRS-2, No. 1, February, 1987, pp. 153-160.

[17] A. A. Girgis and R. B. McManis, "Frequency domain techniques for modeling distribution or transmission networks using capacitor switching induced transients," IEEE Trans. Power Delivery, vol. 4, pp. 1882–1890, July 1989.

[18] M. Nagpal, W. Xu, and J. H. Sawada, "Harmonic impedance measurement using three-phase transients," IEEE Trans. Power Delivery, vol. 13, pp. 272–277, Jan. 1998.

[19] Shumway R.H. and. Stoffer D.S., *Time Series Analysis and Its Applications*, 2000, New York: Springer.

[20] A. de Oliveira, J. C. de Oliveira, J. W. Resende, and M. S. Miskulin, "Practical approaches for AC system harmonic impedance measurements," IEEE Trans. Power Delivery, vol. 6, pp. 1721–1726, Oct. 1991.

[21] W. Xu, E. E. Ahmed, X. Zhang and X. Liu. "Measurement of Network Harmonic Impedances: Practical Implementation Issues and Their Solutions", IEEE Transactions on Power Delivery, pp 210-216 vol. 17, No. 1 January 2002.

[22] E. Clarke. "Circuit Analysis of A-C Power Systems, vol. 1 Symmetrical and Related Components" New York: John Wiley and Sons 1943 (seventh printing –1961).

[23] L. Cristaldi and A. Ferrero, "Harmonic power flow analysis for the measurement of the electric power quality," IEEE Trans. Instrum. Meas., vol.44, pp. 683–685, June 1995.

[24] T. Tanaka and H. Akagi. "A new method of harmonic power direction based on the instantaneous active power in three-phase circuits", IEEE Trans, Power Delivery, vol. 10 pp.1737-1742, Oct. 1995.

[25] P. H. Swart, M. J. Case, and J. D. VanWyk, "On techniques for localization of sources producing distortion in three-phase networks," The Eur. Trans. Elect. Power Eng., vol. 6, no. 6, pp. 391–396, Nov./Dec. 1996.

[26] A. E. Emanuel, "On the assessment of harmonic pollution," IEEE Trans.Power Delivery, vol. 10, pp. 1693–1698, July 1995.

[27] A. M. Dán and Zs. Czira. "Identification of harmonic Sources", 8th International Conference on Harmonic and Quality of the Power IEEE/PES and NTUA, Athens, Greece, pp 831-836, Oct 1998.

[28] W. Xu, "On the validity of the power direction method of identifying harmonic source locations," IEEE Power Eng. Rev., vol. 20, pp. 48–49, Jan. 2000.

[29] C. Li, W. Xu and T. Tayjasanant, "A 'Critical Impedance' - based method for identifying harmonic sources", IEEE Transaction on Power Delivery. Vol. 19. No 2, pp 671-678 Apr. 2004.

[30] K. Srinivasan, "On separating customer and supply side harmonic contributions," IEEE Transactions on Power Delivery, vol. 112, pp.1003–1012, Apr. 1996.

[31] M. Tsukamoto, I. Kouda, Y. Natsuda, Y. Minowa, and S. Nishimura, "Advanced method to identify harmonic characteristic between utility grid and harmonic current sources," in Proc. 8th Int. Conf. Harmonics Quality Power, Athens, Greece, Oct. 1998, pp. 419–425.

[32] E. Thunberg and L. Söder. "A Norton approach to distribution network model for harmonic studies", IEEE Trans, Power Delivery, vol. 14 No. 11, pp.272-277, Jan. 1994.

[33] W. Xu and Y. Liu, "A method for determining customer and utility harmonic contributions at the point of common coupling," IEEE Trans. Power Delivery, vol. 15, pp. 804–811, Apr. 2000.

[34] O. Gonbeau, L. Berthet, J. Javerzac and D. Boudou, "Method to determine contribution of the customer and the power system to the harmonic disturbance", CIRED 17th International Conference on Electricity Distribution Barcelona, 12-15 May 2003.

[35] Testa A., Castaldo D. and Langella R., "Probabilistic Aspects of Harmonic Impedances". IEEE Power Engineering Society Winter Meeting, 2002. Volume 2, 27-31 Jan. 2002, pp. 1076 – 1081

[36] Fuja T. E., Heegard C. D., "Focused Codes for Channels with Skewed Errors". IEEE Transactions on Information Theory. Vol. 36, No 4, July 1990, pp. 773 – 783

[37] Lee Y. and An Q., "Calibration of Time-Skew Error in a M-Channel Time-Interleaved Analog-to-Digital Converter". Proceedings of World Academy of Science, Engineering and Technology. Vol. 2, January 2005, pp. 280-283.

[38] C. Boor, "A Practical Guide to Splines". Applied Mathematical Sciences, Springer, 1994.

[39] IEEE Recommended Practice for Monitoring Electric Power Quality: IEEE Std. 1159-1995.

[40] W. R. Anis and M. M. Morcos, "Artificial Intelligence and Advanced Mathematical Tools for Power Quality Applications: A Survey", IEEE Trans. on Power Delivery, Vol. 17, No. 2, April 2002.

[41] D. D. Sabin, T. E. Grebe, D. L. Brooks, and A. Sundaram, "Rules-based Algorithm for Detecting Transient Overvoltages due to Capacitor Switching and Statistical Analysis of Capacitor Switching in Distribution Systems", IEEE Transmission and Distribution Conference, Vol. 2, 11-16 April 1999, New Orleans, USA, pp. 630-635.

[42] ION Enterprise, Power Measurement, PowerLogic, "ION User's Guide", Transient Detection Module (ION 7650/8600), Canada, 2004.

[43] Alan V. Oppenheim and Ronald W. Schafer, *Discrete-Time Signal Processing*, 2nd Edition. Prentice Hall: Upper Saddle River, NJ, 1999.

[44] R. Dwyer, A. K. Khan, M. McGranaghan, L. Tang, R. K. McCluskey, R. Sung, T. Houy, "Evaluation of Harmonic Impacts from Compact Fluorescent

Lights on Distribution Systems", IEEE Transactions on Power Systems, Vol. 10, No. 4, 1995, pp. 1772-1779.